



**COMPARISON OF PROBABILITY OF ERROR PERFORMANCE FOR
TRUNCATED BESSEL AND BESSEL-GAUSS BEAMS**

MERT BAYRAKTAR

AUGUST 2015

**COMPARISON OF PROBABILITY OF ERROR PERFORMANCE FOR
TRUNCATED BESSEL AND BESSEL-GAUSS BEAMS**

**A THESIS SUBMITTED TO
THE GRADUATE SCHOOL OF NATURAL AND APPLIED
SCIENCES OF
ÇANKAYA UNIVERSITY**

**BY
MERT BAYRAKTAR**

**IN PARTIAL FULFILLMENT OF THE REQUIREMENTS FOR THE
DEGREE OF
MASTER OF SCIENCE
IN
THE DEPARTMENT OF
ELECTRONIC AND COMMUNICATION ENGINEERING**

AUGUST 2015

**Title of the Thesis: Comparison of probability of error performance for
truncated Bessel and Bessel Gauss Beams.**


Submitted by **Mert BAYRAKTAR**

Approval of the Graduate School of Natural and Applied Sciences, Çankaya
University.



Prof. Dr. Halil Tanyer EYYUBOĞLU
Director

I certify that this thesis satisfies all the requirements as a thesis for the degree of
Master of Science.



Prof. Dr. Halil Tanyer EYYUBOĞLU
Head of Department

This is to certify that we have read this thesis and that in our opinion it is fully
adequate, in scope and quality, as a thesis for the degree of Master of Science.



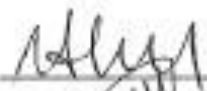
Prof. Dr. Halil Tanyer EYYUBOĞLU
Supervisor

Examination Date: 14.08.2015

Examining Committee Members

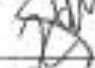
Assoc. Prof. Dr. Nursel AKÇAM

(Gazi Univ.)



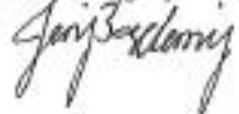
Prof. Dr. Halil Tanyer EYYUBOĞLU

(Çankaya Univ.)



Assist. Prof. Dr. Hüsnü Deniz
BAŞDEMİR

(Çankaya Univ.)



STATEMENT OF NON-PLAGIARISM PAGE

I hereby declare that all information in this document has been obtained and presented in accordance with academic rules and ethical conduct. I also declare that, as required by these rules and conduct, I have fully cited and referenced all material and results that are not original to this work.

Name, Last Name : Mert
: BAYRAKTAR
Signature : 
Date : 14.08.2015

ABSTRACT

Comparison of probability of error performance for truncated Bessel and Bessel Gauss Beams

BAYRAKTAR, Mert

M.Sc., Department of Electronic and Communication Engineering

Supervisor: Prof. Dr. Halil Tanyer EYYUBOĞLU

August 2015,71 pages

In this thesis, probability of error and SNR performances of truncated Bessel and Bessel-Gauss beams in free space optical communication system were compared. Source beams were determined as truncated Bessel and Bessel-Gauss beam. Then, the simulation of propagation of these beams was simulated in MATLAB. This simulation was performed by using random phase screen approach. Random phase screen was used as a model of the turbulent atmosphere in reality. Data symbols were transmitted to receiver side through the random phase screen. To reach the probability of error of this communication system, error counting was applied. By this way, performance comparison of the beams was derived and relative plots were located in this paper.

Keywords: Beam Shaping, Bessel beam, Random Phase Screen.

ÖZ

Kesik Bessel ve Bessel-Gauss Işınlarnn Hata Oranı Performans Karşılaştırılması

BAYRAKTAR, Mert

Yüksek Lisans, Elektronik ve Haberleşme Mühendisliği Anabilim Dalı

Tez Yöneticisi: Prof. Dr. Halil Tanyer EYYUBOĞLU

Ağustos 2015, 71sayfa

Bu tezde, serbest uzay optik sistemlerde kesik Bessel ve Bessel-Gauss ışınlarının hata olasılığı ve sinyal-gürültü oranı performansları karşılaştırılmıştır. Kaynak ışınları kesik Bessel ve Bessel Gauss ışını olarak belirlenmiştir. Bu ışınların ilerleyişlerinin benzetimi MATLAB’da yapılmıştır. Bu simülasyonlar rastgele faz tabakaları modeli kullanılarak gerçekleştirilmiştir. Rastgele faz tabakaları, gerçekteki atmosfer türbülansını modellemek için kullanılmıştır. Veri sembolleri alıcıya bu rastgele faz tabakaları üzerinden gönderilmiştir. Bu haberleşme sisteminin hata olasılığına ulaşmak için hata sayımı uygulanmıştır. Bu yolla, ışınların performans karşılaştırılması çıkarılmış ve ilgili çizimler çalışmada yer bulmaktadır.

Anahtar Kelimeler: Işın Modelleme, Bessel Işını, Rastgele faz tabakaları.

ACKNOWLEDGEMENTS

I would like to express my sincere gratitude to Prof. Dr. Halil Tanyer EYYUBOĞLU for his supervision, special guidance, suggestions, and encouragement through the development of this thesis. Additionally, thanks for the support of Prof. Dr. Yusuf Ziya UMUL during the study.

It is a pleasure to express my special thanks to my family for their valuable support.

TABLE OF CONTENTS

STATEMENT OF NON PLAGIARISM.....	ii
ABSTRACT.....	iii
ÖZ.....	iv
ACKNOWLEDGEMENTS.....	v
TABLE OF CONTENTS.....	vi
LIST OF FIGURES.....	viii
LIST OF ABBREVIATIONS.....	x

CHAPTERS:

1. INTRODUCTION.....	1
1.1. Background	1
1.2. Basics.....	3
1.3. Objectives.....	6
1.4. Organization of Thesis.....	7
2. PHYSICAL IMPLEMENTATION OF THE SYSTEM.....	9
2.1. Interface	9
2.2. Transmitter	10
2.3. Optical Design	15
2.4. Receiver.....	15
2.5. Physical Design Considerations.....	15
3. ATMOSPHERE.....	18
3.1. Link Budget Analysis.....	18
3.2. Attenuation.....	20
3.3. Scintillation.....	20
3.4. Scattering.....	23
3.5. Random Phase Screen Derivation and Its Application for Selected Beam Types.....	24

3.6.	Power Settings of Beam Types.....	30
3.7.	Signal to Noise Ratio Derivation.....	31
4.	ANALYSIS WITH RESPECT TO SOURCE SIZE	33
4.1.	Pe, SNR, Received Power Analysis of Bessel Gauss Beam when $\alpha_s = 3.2\text{cm}$	33
4.2.	Pe, SNR, Received Power Analysis of Bessel Gauss Beam when $\alpha_s = 6.5$	36
4.3.	Pe, SNR, Received Power Analysis of Bessel Gauss Beam when $\alpha_s = 7.9$	38
5.	ANALYSIS WITH RESPECT TO ORDERS.....	41
5.1.	Pe Analysis of Bessel Gauss Beam With Respect to Order.....	41
5.2.	SNR Analysis of Bessel Gauss Beam With Respect to Order.....	43
5.3.	Received Power Analysis of Bessel Gauss Beam With Respect to Order.....	45
6.	ANALYSIS OF BESSEL BEAM WITH RESPECT TO ORDERS.....	48
7.	CONCLUSION.....	50
	REFERENCES.....	52
	APPENDICES.....	R1
A.	CURRICULUM VITAE.....	A1

LIST OF FIGURES

FIGURES

Figure 1	Transceiver block diagram	1
Figure 2	Optical link simulation model including atmospheric turbulence.....	7
Figure 3	Designed FSO transmitter photo.....	11
Figure 4	Basic lens design.....	12
Figure 5	Optical system design.....	13
Figure 6	Beam size vs propagation distance.....	14
Figure 7	Basic lens design for receiver side	14
Figure 8	Receiver photo.....	15
Figure 9	Ground plane view between current paths	16
Figure 10	Current path drawings.....	16
Figure 11	Representation of Geometric Loss at the receiver.....	18
Figure 12	Pe behavior of Bessel Gauss Beams (BGBs) with respect to structure constant when $\alpha_s = 3.2\text{cm}$ for different orders.....	33
Figure 13	SNR behavior of BGBs with respect to structure constant when $\alpha_s = 3.2\text{cm}$ for different orders.....	34
Figure 14	Received power of BGBs with respect to structure constant when $\alpha_s = 3.2\text{cm}$ for different orders.....	35
Figure 15	Pe behavior of BGBs with respect to structure constant when $\alpha_s = 6.5\text{cm}$ for different orders.....	36
Figure 16	SNR behavior of BGBs with respect to structure constant when $\alpha_s = 6.5\text{cm}$ for different orders.....	37
Figure 17	Received power of BGBs with respect to structure constant	37

when $\alpha_s = 6.5\text{cm}$ for different orders.....

FIGURES

Figure 18	Pe behavior of BGBs with respect to structure constant when $\alpha_s = 7.9\text{cm}$ for different orders.....	38
Figure 19	SNR behavior of BGBs with respect to structure constant when $\alpha_s = 7.9\text{cm}$ for different orders.....	39
Figure 20	Received power of BGBs with respect to structure constant when $\alpha_s = 7.9\text{cm}$ for different orders.....	40
Figure 21	Pe performance of zero order BGB for different source sizes...	41
Figure 22	Pe performance of first order BGB for different source sizes.....	42
Figure 23	Pe performance of second order BGB for different source sizes	42
Figure 24	SNR comparison of zero order BGB with different source sizes	43
Figure 25	SNR comparison of first order BGB with different source sizes	44
Figure 26	SNR comparison of second order BGB with different source sizes	44
Figure 27	Power comparison of zero order BGB with different source sizes	45
Figure 28	Power comparison of first order BGB with different source sizes	46
Figure 29	Power comparison of second order BGB with different source sizes	46
Figure 30	Probability of error comparison of Bessel Beams with different orders	48
Figure 31	SNR comparisons of Bessel Beams with different orders	49

LIST OF ABBREVIATIONS

FSO	Free Space Optics
RPS	Random Phase Screen
BGB	Bessel-Gauss Beam
TBB	Truncated Bessel Beam
GB	Gauss Beam
BER	Bit Error Rate
MAC	Media Access Controller
GMII	Gigabit Media Independent Interface
VCSEL	Vertical Cavity Surface Emitting Laser
APD	Avalanche Photo Diode
Pe	Probability of Error

CHAPTER 1

INTRODUCTION

1.1 Background

Bit error rate (BER) of a free space optical system (FSO) is worth carrying out a research on it. Scientists are also interested in this topic. So, BER performance analysis under different conditions is very important for FSO systems. In [1], BER performance of a FSO system is examined by considering scintillation, spreading, and wandering according to wavelength and source size differences. Instead of usage of a single detector, array detectors are also studied in [2,3] and it is stated in [3] that array receiver shows better performance as compared to single detector. In addition to this, different features of a FSO system are analyzed for different atmospheric conditions. Scintillation effect over BER was studied in [4]. Non-Kolmogorov turbulence is applied to the study in [5] and it is observed that scintillation decreases under this atmospheric model. In [6], FSO works in K-distributed turbulence and performance analysis with Differential Phase Shift Keying (DPSK) was studied. Low Density Parity Check Code (LDPC) shows better performance in Gamma-Gamma distributed atmosphere as compared to Reed Solomon Code in the analysis of [7]. LDPC were applied to a hybrid FSO system in [8] to observe the effect of adaptive code modulation. Additionally, a hybrid FSO experiment was set up in [9] to see the reduction of atmospheric effects on hybrid systems. Another physical experiment was demonstrated in [10] and orbital angular momentum was applied to the system. BER of FSO system was studied by applying different techniques. Changing the modulation type improves the BER of optical communication systems. From this point, effect of Binary Phase Shift Keying (BPSK) was studied under weak to strong turbulence [11]. BER comparison of On-Off keying (OOK), Differential Phase Shift

Keying (DPSK), and Differential Quadruple Phase Shift Keying (DQPSK) was carried out with and without Space Diversity Reception Technique (SDRT) [12]. Another way to improve BER performance of FSO system is beam shaping. Truncated Mathieu beam was propagated through ABCD paraxial optical system in [13] and it was detail analyzed in [14] using Collings Formula. Utilizing aperture averaging BER analysis of fully coherent and Gaussian Schell beam was obtained in [15]. Scientists are interested in Bessel like beams. Super-Gaussian Bessel beam was introduced to the literature in [16]. Bessel-Gauss Beam was introduced and propagation of this type of beam was first analyzed in [17]. Cylindrical-Sinc beam which is half order Bessel beam was introduced in [18]. Bessel Beam was obtained by solving Helmholtz equation in [19]. It was explained in [20] that Bessel beam is a standing wave in a cylindrical system. Bessel beam was created as truncated Bessel and Bessel-Gauss form, because Bessel beam need infinity energy. In [21], using a couple of Distributed Bragg Reflectors (DBR), Bessel beam was generated. For generating spiraling first order Bessel Beams, hologram and axicon are used in [22], in addition to hologram and axicon, an aperture is placed between them to generate higher order Bessel beam. Special lens system was designed in [23] to obtain an elliptical Bessel beam. Another experimental setup was established in [24] and March-Zehnder interferometer was used to see the experimental results. However, Bessel beam was generated practically, [25] show that this beam turns to Gaussian beam after propagation. But during the propagation through the liquid Bessel beam shows its self-reconstruction behavior in [26]. Modified Bessel-Gauss beam which is another type of Bessel beam was studied in [27] and the results were obtained with respect to different structure constants C_n^2 and different Bessel orders. Similar analysis was performed for truncated Bessel beam in [28] and behavior of the beam with respect to the atmosphere was analyzed. In this study, it is pointed out that intensity at receiver is affected by wavelength, beam topological charge, and beam waist. These types of beams show different performance for different distances. That's why; far field and near field analysis seems interesting. Analytical and

numerical analysis of Bessel Modulated Gauss beam with quadruple radial dependence was carried out in [29] and beam quality factor M^2 was derived for far field. As opposed to far field, near field analysis of truncated Bessel beam for different orders was performed in [30]. To generalize the truncated beams, truncation parameter σ and propagation factor m^2 were studied for flattened Gaussian and cosh-Gaussian beams [31]. Propagation factor of Bessel-Gauss beam was derived in [32]. Propagation parameter and Kurtosis parameter which gives an idea about the sharpness of the beam profile was derived in free space in [33]. In addition to propagation parameter, power in bucket analysis was done in [34] for different beam parameters. Kurtosis parameter of elegant Hermite Gaussian beam and Laguerre Gaussian beam was derived in [35]. It is identified in [36] that K_x is related with the uniaxial crystals for the Gaussian flat topped beam. It is shown in [37] those kurtosis parameter and beam propagation factors are directly proportional to bandwidth of broadband Gaussian beam. It is clearly identified in [38] that using positive and negative axicons propagation parameter increases. As a combination, different kurtosis parameters are shown in [39] for different types of beams.

Signal to noise ratio (SNR) bounds of selected beams were analyzed by the author in [40] and it is stated that small source sized beams shows the best performance.

In this thesis, BER, received power, and SNR comparisons of truncated Bessel and Bessel-Gauss beams are studied. By comparing detected symbols after random phase screen and transmitted symbols, errors are counted. By this way, BER value of the system is obtained. Additionally, received power is measured after 5500 meter link distance. Finally, considering shot and thermal noise, SNR of the system is derived.

1.2 Basics

Free space optics is one of the most important communication systems in our developing world. That's why, scientists work on these systems to improve their

performance of these systems. Performance of a FSO system can be defined as increasing the range, decreasing BER, and increasing data speed. To provide these improvements, encoding, changing modulation types, and beam shaping can be applied.

Before all these improvements, basics and working principle of a FSO system should be analyzed.

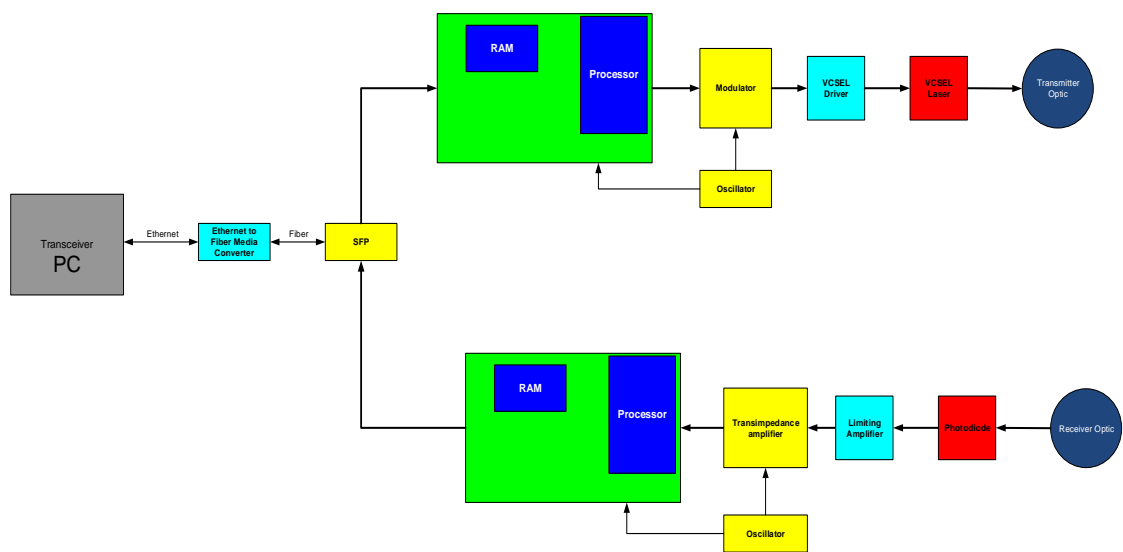


Figure 1 Transceiver block diagram

A FSO system includes these parts which are showed in Fig.1. Mainly, parallel data is converted into a serial bit stream by using parallel to serial converter. Then, serial data stream is fed to the laser driver. Laser driver triggers the laser and laser performs OOK modulation which means that light is on when data is logic 1 or light is off when data is logic 0. At this point, electro-optic conversion occurred meaningfully data is converted from electrical to optical form. Lasers must be chosen considering its switching speed, operating wavelength, beam divergence angle. Firstly, data speed is very important because it is impossible to use all lasers different speed systems. Laser's switching speed should be as fast as the transition speed. If the laser is not fast enough for data speed, laser will burn out. In laboratory

experiments, laser diode of a laser pointer can work up to 10 Mbps but when the speed reaches to 1Gbps level, laser burns out. Then, laser is chosen as Vertical Cavity Surface Emitting Laser (VCSEL) since this type of lasers is designed for higher data speeds. On the other hand, this laser selection is a trade-off. However, VCSELs can operate in higher data rate; optical output power of VCSELs is less as compared to laser diodes. Therefore, communication distance decreases when data speed increases.

Next important thing to determine the laser is wavelength, because operating wavelength of a laser should be the same as photo receiver'. It must also be chosen by considering atmospheric affect over the wavelength. In this thesis, wavelength of the practical system is chosen as 850 nm and wavelength of simulation part is chosen as 1550 nm.

Finally, beam divergence angle of a laser diode is crucial, because all photons emitted from laser should be on the clear aperture of the collimator lens. If beam divergence angle is so much to collect all emitted photons over the collimator lens, then the output power efficiency of a transmitter system decreases. Meaningfully, the measured optical power after collimator will be less than output power of the laser if beam divergence of a laser is larger than critical angle.

Unfortunately, light does not propagate in small size during the transmission medium. Lasers spread the light with a beam divergence angle. Divergence of data with the light should be prevented by an optical lens system. From now on, light propagates nearly parallel to propagation axis which is named as z . During the propagation atmosphere reduces the intensity of the light. When photons fall over the receiver aperture, receiver lens focuses the light over photo receiver. A focusing asymmetric doublet lens is frequently used in FSO systems. This type of lens is used, because photons must be focused on the photo receiver to create current.

This photo receiver creates current directly proportional to photons on it. Meaningfully, photo receiver creates more current if number of photons increases.

Data is converted from optical form to electrical form utilizing opto-electronic conversion. Generated current by photodiode is shown below

$$\langle I_G \rangle = M_f R_f \langle P_r(L) \rangle \quad (1.1)$$

where M_f is the multiplication factor, R_f is the responsivity of the photodiode, $\langle \rangle$ refers to averaging operation, and $P_r(L)$ is instantaneously received power. Optical receivers can be grouped as phototransistors and photodiodes. Main differences between phototransistors and photodiodes are data speed and decision accuracy. Photodiodes operate in higher data speed as compared to phototransistors. On the other hand, phototransistors are more reliable in terms of decision accuracy.

1.3 Objectives

The main purpose of this study is to derive the BER of an FSO system using Bessel-Gauss and truncated Bessel Beams. In both cases, output power of the system is stabilized as 21mW. Atmosphere types in the literature are studied such as von Karman and Kolmogorov. Generated beams are propagated through Random Phase Screens (RPSs), which are combination of von Karman and Kolmogorov atmosphere model, to simulate the atmosphere. These screens decrease the intensity and changes the phase of the beam like atmosphere does. Probability of error of these two beams for an FSO system is calculated for different source size and Bessel orders. Output power is set to 21mW and then effects of source size differences are observed. By comparing the transmitted and received symbols Pe is calculated. Moreover, an FSO system is designed with support of current project.

Figure 2 illustrates the simulation environment of free space optical link. At the transmitter side, $u_{s1,2}$ represents the source beam expression. System operates 21 mW emitted power, P_s with different source sizes which are explained in the power

analysis. At the receiver side, after 5500 meter distance, receiver aperture is the same for all conditions. Received power $P_r(L)$ and SNR values are calculated using shot and thermal noise in addition to received power. Atmospheric fluctuations between transmitter and receiver are modelled utilizing random phase screen approach. P_e of the system for different source and Bessel order setting is calculated. Random symbols are transmitted applying 2-Amplitude Shift Keying (2-ASK), received symbols are obtained with some errors due to the atmospheric fluctuations. Atmospheric fluctuations change the power of the received beam. Therefore, applying threshold detection at the receiver side can cause bit errors. After obtaining received symbols, transmitted and received bit streams are compared and bit error rate value is calculated.

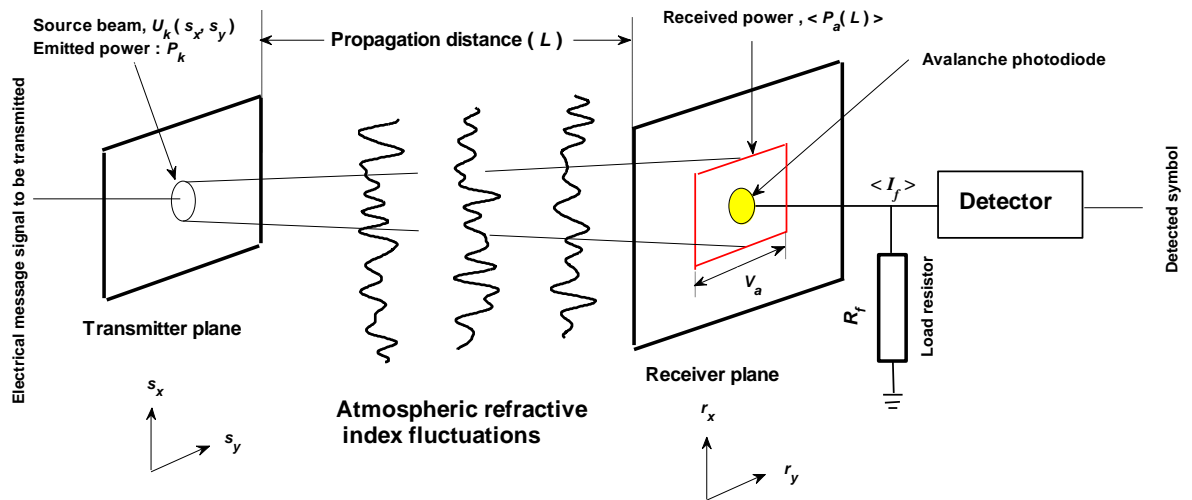


Figure 2 Optical link simulation model including atmospheric turbulence[40]

1.4 Organization of the Thesis

This thesis is divided into seven chapters. All analysis are studied to obtain P_e , SNR, and received power. These results are used to make a comparison in terms of source size and orders.

Chapter 1 is an introduction and background for free space optics links and objectives of this thesis.

Chapter 2 involves physical implementation of the system dividing into parts such as interface, transmitter, optical design, and receiver part.

Chapter 3, explains the atmospheric affects over the beam. Additionally, received field derivations are studied in this chapter.

In Chapter 4, P_e , SNR, and received power analysis is studied and comparison of beams are performed for different source sizes.

In Chapter 5, P_e , SNR, and received power analysis is studied and comparison of beams are performed for different beam orders.

Chapter 6 includes the P_e , SNR, and received power results of Bessel Beam for different atmospheric conditions.

Chapter 7 has the conclusion part.

CHAPTER 2

PHYSICAL IMPLEMENTATION OF THE SYSTEM

2.1 Interface

Open System Interconnection (OSI) layers are introduced to divide the system into logical parts. A classical FSO system includes parts in physical layer, data link, and network layer. FSO systems are designed to set input/output (I/O) ports as Small Form Pluggable (SFPs) because these systems are generally used in backbone which used with routers. Output of these routers is fiber coupled so FSO systems are generally designed with SFP or Small Form Factors (SFF). To realize the backbone, practical work in this thesis is designed fiber coupled. Data which is transmitted from the computer is converted into optical form by using MC200CM media converter. This media converter operates in gigabit Ethernet up to 550 meter distance with a SC connector fiber cable. Operating wavelength of this media converter is 850 nm. Since wavelength of this device is 850 nm, operating wavelength of the SFP must be the same as media converter. Bearing in mind that information, SFP is chosen as HFBR 5912ez from Avago Technologies. This component creates electrical signal with respect to the incoming data in optical form. This differential data is fed to the HDMP 1646a serializer - deserializer (SERDES) with Phase Lock Loop (PLL). This component converts data into parallel form. PLL is the one of the most crucial feature because PLL clears the phase difference of the signals. If PLL is not used in Ethernet applications, system fail since Ethernet is a kind of synchronous communication protocol. Fundamental frequency of the system is 125 MHz for Gigabit Ethernet applications and phase locking is performed on this frequency.

Next, parallel outputs of the system are fed to processor directly. These parallel data pins are in the form of Gigabit Media Independent Interface. Each pin is responsible for different missions. For transmitter side, eight pins assigned as TX data pins and called as TXD. GTXCLK pin generates clock signal for gigabit Ethernet as 125 MHz. For 10 and 100 Mbps systems, TXCLK pin generates clock signal respectively 2.5 MHz and 25 MHz. TXEN pins are responsible for enabling the transmission. TXER pin is active when an error occurs during the communication. At the receiver side, symmetrically eight pins are reserved for RX signals. Because gigabit Ethernet has clock recovery, RXCLK pin generates clock signal from incoming data. RXDV is active when received data is valid. RXER is similar to TXER which defines the error during communication. CS and COL pins are used in half duplex systems and they refer respectively carrier sense and collision detect. To establish a communication using GMII interface, interface system should be control utilizing management pins. These management pins are management interface clock (MDC) and management I/O pins (MDIO).

This processor gives the MAC address to the device. Cheapest way to give MAC address is to use MAC integrated circuits of Microchip. This MAC address is loaded into the RAM of the processor and signal is converted into the suitable form for modulator.

2.2 Transmitter

From this point data is ready to apply to the laser driver. Laser driver behaves as a constant current source for the laser. These drivers prevent the unwanted noise at the transmitter side. In the practical view, MAX 3656 was chosen as the laser driver, because this laser driver has a wide range of modulation current from 10mA to 85 mA. Output voltage is suitable for the laser which is PH85-D2P0U4 because of its high output optical power and high data speed. MAX 3656 laser driver and PH85-D2P0U4 VCSEL laser are soldered on the PCB as shown below.

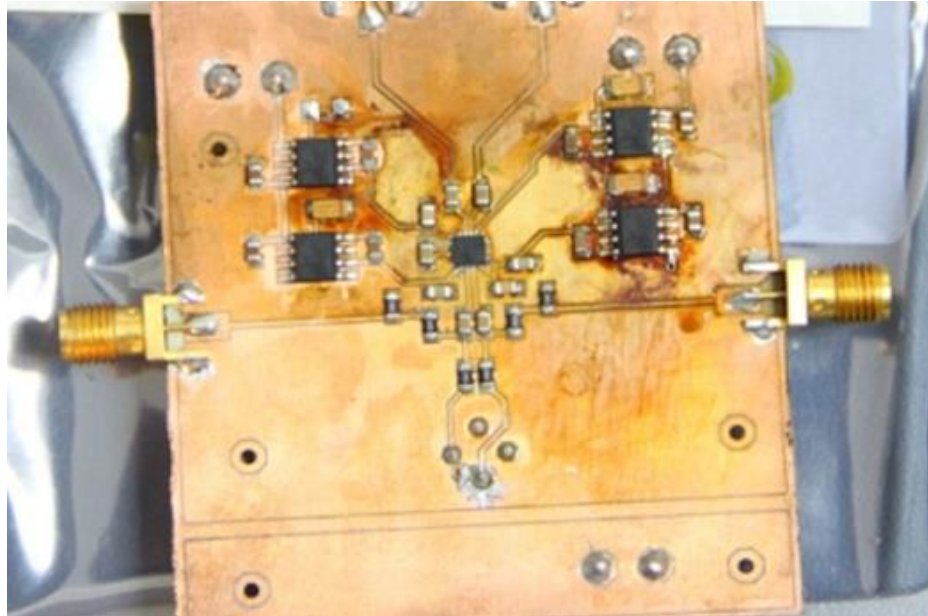


Figure 3 Designed FSO transmitter photo

Laser driver triggers the laser by performing on-off keying (OOK). Meaningfully, light is on when data is logic 1, light is off when data is logic 0. This process occurs 1 billion times in a second. Considering that human eyes do not recognize fluctuations more than 40 times in a second, this speed is so fast to recognize. Wavelength of the laser is chosen as 850 nm to see the light via mobile camera. Since, it is mentioned in [41] that this wavelength shows the best atmospheric performance. At this point, data is converted from electronic form to optical form by performing electro-optic conversion.

Next step is to select and establish the optical setup of the system.

2.3 Optical Design

Lasers have some beam divergence angle at the optical output. Photons generated by laser resonator are not collimated not to spread. To collimate these photons optical collimator is used. Optical collimator basically includes a thin lens. Main idea behind the collimators is based on the optics physics laws. The idea is that if you put the

light source to focal length of the lens, light is focused at infinity. Unfortunately, this idea is theoretically possible. In the practical approach, light always diverges. That's why; receiver lens of the system has larger radius. By choosing the collimator, there are some important features to be considered such as operation wavelength, beam divergence of the laser, critical angle, numerical (NA) and clear aperture (CA) of the lens. Firstly, optical lenses have anti-reflector coating to apply an optical filter. So, it is not possible to use all lenses for all applications. Laser and the lens should work at the same wavelength to minimize optical power loose at the transmitter and affect the receiver from unwanted light. Rest of the parameters must be considered together when designing the optical system. First, beam divergence is defined as θ and critical angle of the lens is defined as θ_c . Generally $\theta < \theta_c$ identity must be hold because if beam divergence angle larger than the critical angle, all photons emitted from the laser are not collimated. Meaningfully, NA represents the incoming light capacity of the lens and CA represents the active area of the lens. If $\theta_c < \theta$, photons exceeds the NA and CA. Hence, output power of the laser is not measured from the output of the lens. Ideal lens design can be formed by using trigonometric view located as shown in Fig.4.

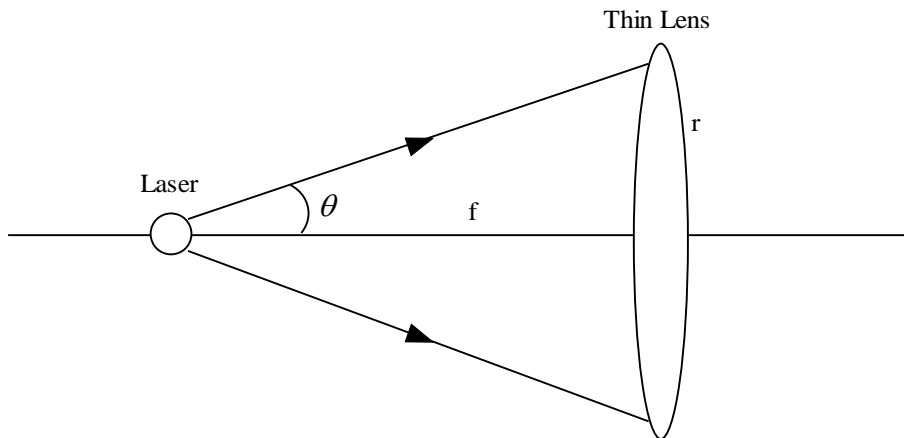


Figure 4 Basic lens design

Here r is the radius; f is the focal length of the lens. In Fig.4, the laser is put to the focal length of the lens to collimate the light at infinity. r and f values are located in datasheet of the lens. When the laser is determined, radius, critical angle, and numerical aperture of lens can be taken into account. Beam divergence of the laser which is used in this design is 2 degrees. Collimator of the system was chosen according to following trigonometric identity.

$$\theta \leq \arctan\left(\frac{r}{f}\right) \quad (2.1)$$

Bearing in mind that the trigonometric relation above, the next thing will be performed is selecting the lens. For our case the collimator was chosen as LT110P-B, which can be used with $\phi 5.6$ and $\phi 9mm$. According to the calculations, it is clear that this lens and laser diode is suitable for each other.

Optical design and in the laboratory is shown in Fig.5 .

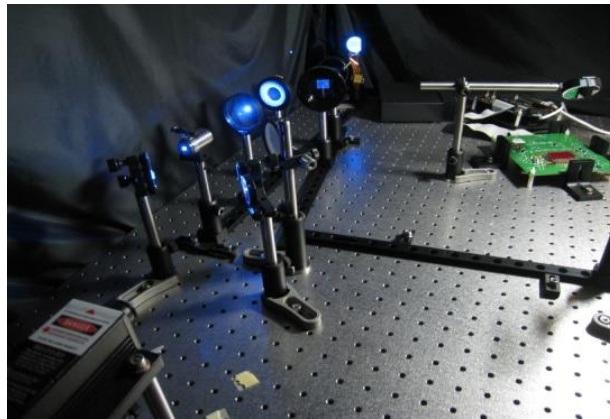


Figure 5 Optical system design

As it is defined in [42], beam size at the receiver is calculated as

$$\alpha_r = \left(\frac{k^2 \alpha_s^4 F_s^2 - 2k^2 \alpha_s^4 F_s z + 4F_s^2 z^2 + k^2 \alpha_s^4 z}{k^2 \alpha_s^2 F_s^2} \right)^{1/2} \quad (2.2)$$

where α_s is the source size, k is the wave number, F_s refers to focusing parameter, and z is the link distance. It can be understood from the above equation that beam spreads more when source size decreases. To prevent this spreading, beam size at the transmitter is made larger using beam expander. Chosen beam expander from Thorlabs “BM03-M-B” is suitable with the collimator output. This beam expander multiplies input beam size by three and in the end of definition of beam expander, “B” indicates the anti-reflector coating of the lens which is 650-1050 nm [43]. By this way, smaller receiver aperture can be used at the receiver side. Output of the collimator is 9.7 mm and after beam expander output beam is 2.91 cm. It is simulated in MATLAB and result shows that this system can operate up to approximately 3 km as shown below.

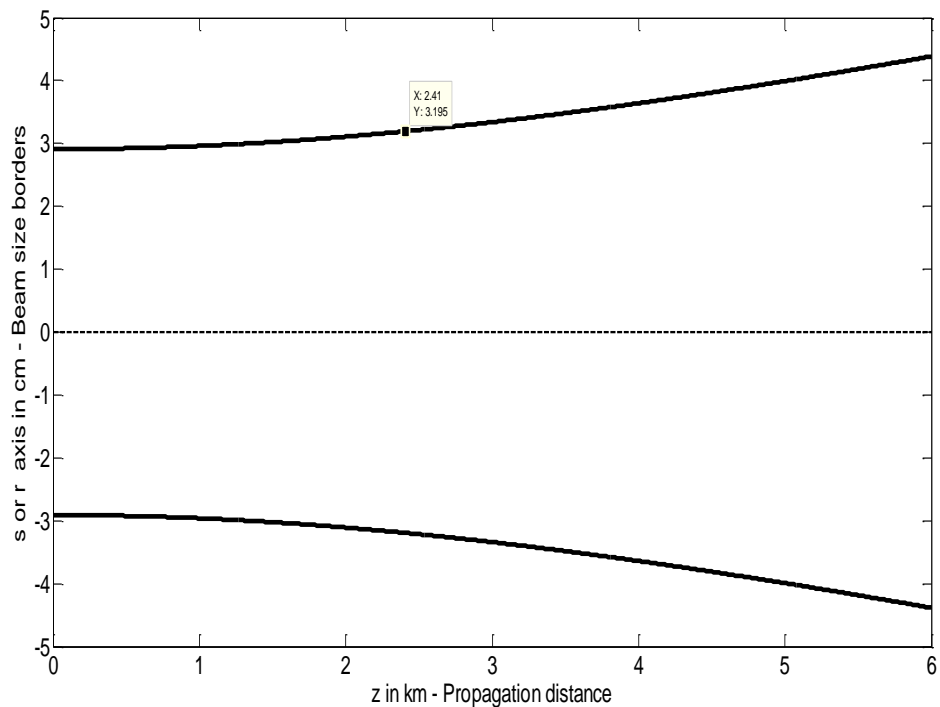


Figure 6 Beam size vs propagation distance

At the receiver side similar optical rules are applied to focus photons over the photodiode.

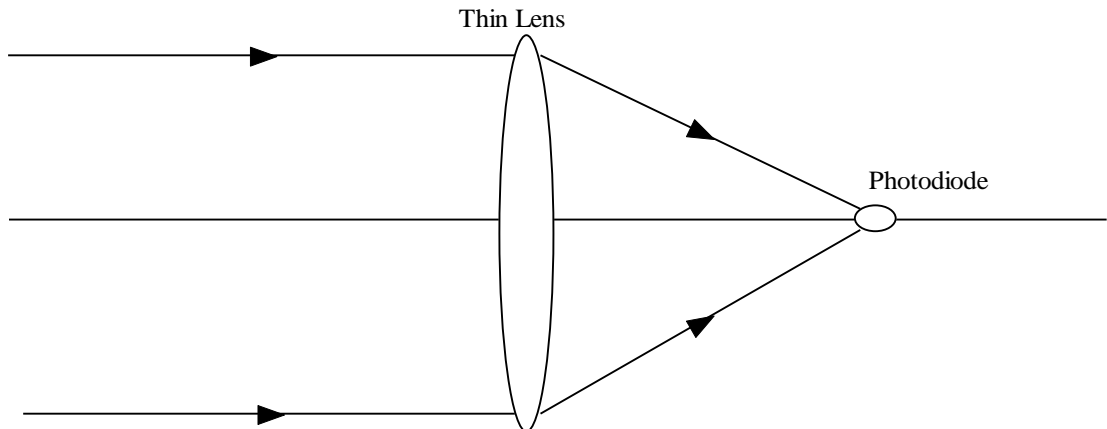


Figure 7 Basic lens design for receiver side.

As it is shown in Fig.7, photons as much as caught should be focused on the photodiode. As an optical part of the receiver, AC508-75-B achromatic doublet lens is used, because of the same operating wavelength and low focal length which is equal to 7.5 cm [44].

2.4 Receiver

In the receiver design first chosen component is the photodiode because of wavelength and operating data speed of the system. To satisfy the wavelength and data speed, ADP210 is chosen. This module operates up to 2.5 Gps and main response is located at 850 nm. As a TransImpedance Amplifier (TIA), current coming from the photodiode is fed to resistor to obtain voltage. Next, output of this stage is fed to limiting amplifier MAX 3748. Then, this system is connected to the interface circuit. Receiver circuit design is located in Fig.8.



Figure 8 Receiver photo

2.5 Physical Design Considerations

During the layout design of these circuits, high frequency circuit design techniques are applied. First, all the paths are isolated via ground plane. Ground plane minimizes the radiation of current paths. If ground plane is not used in high frequency circuits, current paths behave as an antenna. These antennas cause electromagnetic interference on the circuit and signals become meaningless. Secondly, differential signal paths should be symmetric to each other as it is shown below.

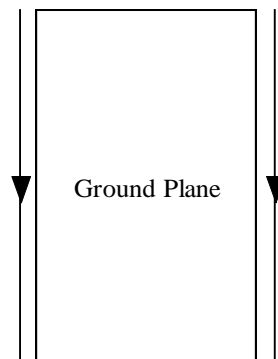


Figure 9 Ground plane view between current paths

Third important thing to design layout for high frequency systems is corners of the signal paths. Designer should be avoided to make 90° turns because standing wave ratio increases and signal power decreases. For better performance, it is better to make to 45° turns as it is done in this thesis. Desired and unwanted turns are shown in Fig.10.

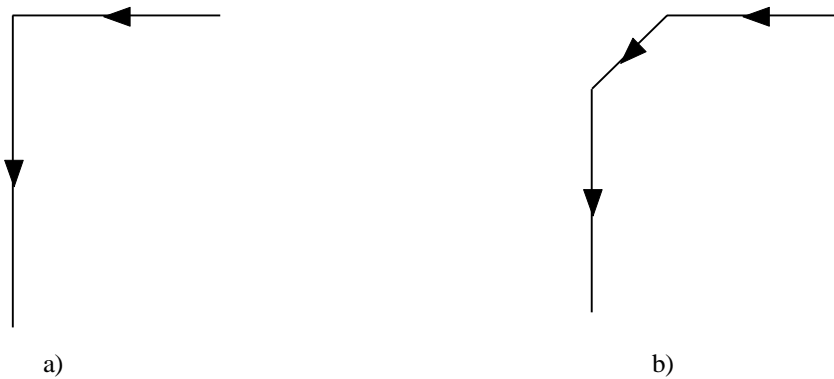


Figure 10 Current path drawings

It is avoided to turn 90° as in part a). In part b), an example wanted turn is shown. Fourth point is to filter the supply voltage of circuits from the noise. Even if, DC seems stable, it has approximately 5% fluctuations in terms of voltage and current. To eliminate DC from these fluctuations, $100\ \mu\text{F}$ capacitor is used because capacitor becomes short circuit in AC. Since, these fluctuations behave as AC signal capacitor is ideal for this filtering. If this filtering does not apply, system output changes with respect to the fluctuations. Next important thing for high frequency circuits is the physical packets of resistors and capacitors. Physical dimensions of circuit components should be as small as possible. If large size components are used, these components also cause interference because their surfaces increase the radiation. In this thesis, resistors and capacitors with 0850 and 1206 packets are used.

CHAPTER 3

ATMOSPHERE

3.1 Link Budget Analysis

Link budget analysis is the basic concept which gives idea whether communication system works or not. Defining fade margin, basic link budget can be calculated as below

$$F_m = P_{Tx} - A_l - G_l + G_{Rx} \quad (3.1)$$
$$F_m > R_s$$

where P_{Tx} is optical output power of the laser, A_l is power loss during the propagation in the atmosphere, G_l is geometric loss because beam diverges and all the photons cannot be caught by the receiver aperture, R_s is receiver sensitivity, and G_{Rx} refers to receiver gain. The power out of the receiver aperture causes geometric loss.

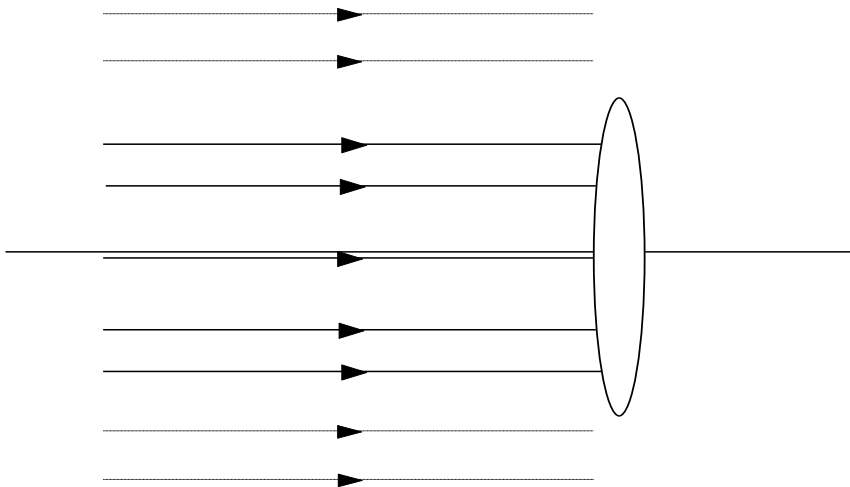


Figure 11 Representation of Geometric Loss at the receiver

In Fig.11, dashed rays are not focused over the receiver that's why these rays are thought as geometric loss.

Finally, beam at the receiver is defined as G_{Rx} . Here, this calculation should be greater than the receiver sensitivity threshold value. If this fade margin remains under the receiver sensitivity, receiver does not detect any bits. Below dependence of A_l to lose per km and distance is given as

$$A_l = L_k d \quad (3.2)$$

where L_k refers to loss per km and d defines the distance. At this point L_k is dependent on the atmospheric conditions. The best performance is seen in clear weather with power decrement of -3 dB/km. As opposed to clear weather, approximately -18 dB/km lose can be measured in heavily foggy weather. But these amounts of loses are valid when Gauss Beam is used as in commercial systems. For the practical system in this study, $P_{Tx} = 5\text{mW}$ (6.9 dB), $G_l \sim 6$ dB, and multiplication factor of receiver amplifier 100 which is equal to 20 dB because avalanche photodiode (APD) is used. Receiver sensitivity of this APD is -30 dB. Arranging the first line of Eq.3.1 and Eq.3.2 it is obtained that

$$d = \frac{P_{Tx} - R_s - G_l + G_{Rx}}{L_k} \quad (3.3)$$

When numerical values are substituted in Eq. 3.3 and maximum operating distance can be calculated as 3.03 km. It means that this system operates up to 3 km under clear weather. If the conditions are kept the same except atmospheric loss per km, effect of atmospheric turbulence is seen easily. For a heavy foggy day, this system operates up to 500 meters from the calculations. The practical system was tested in clear weather with the distance of 100 meters.

There are some atmospheric effects which cause the loss such as attenuation, scintillation, and scattering. Below part is mainly studied in [45].

3.2 Attenuation

This part is studied in [45]. Basically, attenuation can be defined as power reduction. For FSO communication systems, attenuation is caused by aerosols in the atmosphere. Attenuation from the aerosols is defined as

$$A = \int_0^r \alpha(r) dr \quad (3.4)$$

where r is the distance between transmitter and receiver and $\alpha(r)$ is the specific attenuation constant which implies that attenuation occurring in unit distance. This constant can be divided into two parts as

$$\alpha(r) = \alpha_o(r) + \alpha_w(r) \quad (3.5)$$

where $\alpha_o(r)$ is attenuation constant caused by oxygen and $\alpha_w(r)$ is the attenuation constant caused by water vapor. These two variables are dependent on the atmospheric conditions. That's why $\alpha_o(r)$ is represented in three different equation forms depending on the frequency of the aerosols. $\alpha_w(r)$ is also another atmosphere dependent parameter which increases in foggy and rainy weather. In foggy and rainy weather, humidity increases. Humidity is directly proportional to amount of water vapor hanging on the air. As a result, beta is heavily dependent on the atmospheric turbulence. Another atmospheric effect over beam propagation is stated below.

3.3 Scintillation

Scintillation is the intensity fluctuations over received signal caused by the atmosphere. Scintillation index is defined in [46] as

$$m^2 = \frac{\langle I^2 \rangle}{\langle I \rangle^2} - 1 \quad (3.6)$$

here $\langle \rangle$ denotes the averaging operation and I is the intensity of the beam which is computed as

$$I = UU^* \quad (3.7)$$

where U is the field at any point. Scintillation is added to the received signal as noise. It also affects the receiver performance to detect the transmitted symbol. To calculate the scintillation for selected beam types, starting point is Huygens-Fresnel integral like the defined form in Random Phase Screen. Received field of Bessel Gauss beam using Huygens-Fresnel integral becomes

$$u_r(r, \phi_r, z=L) = \frac{A_c \exp(jkL)}{1+2j\alpha L} \exp\left[-\frac{ja_B^2 L + 2\alpha k^2 r^2}{2k(1+2j\alpha L)}\right] J_0\left(\frac{a_B r}{1+2j\alpha L}\right) \quad (3.8)$$

after integral solution of Huygens-Fresnel integral by using Eq.3.937.1, Eq.3.937.2, Eq. 6.633.2 or Eq.6.633.4 in [47]. Used equations in these references are

$$\int_0^{2\pi} dx \exp[p \cos x + q \sin x] \exp[-jmx] = 2\pi \frac{p - jq}{p^2 + q^2} \frac{1}{m/2} I_m \sqrt{p^2 + q^2} \quad (3.9)$$

$$\begin{aligned} \int_0^{2\pi} d\phi_s \exp[-ja \cos \phi_s - \phi_r] \exp[-jmx] &= 2\pi (-1)^m I_m(ja) \exp[-jm\phi_r] \\ &= 2\pi (-j)^m J_m(a) \exp[-jm\phi_r] \end{aligned} \quad (3.10)$$

$$\int_0^\infty dx \exp[-ax^2] J_m(px) I_m(qx) x = \frac{1}{2a} \exp\left(\frac{q^2 - p^2}{4a}\right) J_m\left(\frac{pq}{2a}\right) \quad (3.11)$$

Next, $H(r, \phi_r, \kappa, \phi_\kappa, \eta)$ function is derived using Eq.3.8 as

$$H(r, \phi_r, \kappa, \phi_\kappa, \eta) = \frac{k^2 \exp[jk(L-\eta)]}{2\pi(L-\eta)} \exp\left[\frac{jkr^2}{2(L-\eta)}\right] \int_0^\infty \int_0^{2\pi} dr_1 d\phi_1 u_r(r_1, \phi_1, z=L-\eta) \exp[j\kappa r_1 \cos(\phi_1 - \phi_\kappa)] \exp\left\{\frac{jk}{2(L-\eta)}[r_1^2 - 2r_1 r \cos(\phi_1 - \phi_r)]\right\} \quad (3.12)$$

where κ and ϕ_κ demonstrates amplitude and angular orientation of spatial frequency. Substituting Eq.3.8 to Eq.3.12, $H(r, \phi_r, \kappa, \phi_\kappa, \eta)$ for general order of Bessel Gauss beam becomes

$$H(r, \phi_r, \kappa, \phi_\kappa, \eta) = jk \exp\left[\frac{j\kappa r(1+2j\alpha\eta)}{1+2j\alpha L} \cos(\phi_\kappa - \phi_r)\right] \exp\left[-\frac{0.5j\kappa^2(1+2j\alpha\eta)(L-\eta)}{k(1+2j\alpha L)}\right] \times J_0\left\{\frac{a_B[\kappa^2(L-\eta)^2 - 2k\kappa r(L-\eta)\cos(\phi_\kappa - \phi_r) + k^2 r^2]^{1/2}}{k(1+2j\alpha L)}\right\} / J_0\left(\frac{a_B r}{1+2j\alpha\eta}\right) \quad (3.13)$$

Next, scintillation index $m^2(r, \phi_r, L)$ of a single position marked with coordinates of r and ϕ_r on a receiver far away L from the source is calculated as below

$$m^2(r, \phi_r, L) = 4\pi \int_0^L d\eta \int_0^\infty \kappa d\kappa \int_0^{2\pi} d\phi_\kappa \operatorname{Re} \left[\frac{H(r, \phi_r, \kappa, \phi_\kappa, \eta) H^*(r, \phi_r, \kappa, \phi_\kappa, \eta) + H(r, \phi_r, \kappa, \phi_\kappa, \eta) H(r, \phi_r, -\kappa, \phi_\kappa, \eta)}{H(r, \phi_r, \kappa, \phi_\kappa, \eta) H(r, \phi_r, -\kappa, \phi_\kappa, \eta)} \right] \Phi_n(\kappa) \quad (3.14)$$

where $\Phi_n(\kappa)$ refers to the specific spectrum which is used to define the turbulent propagation medium. By the setting $\Phi_n(\kappa)$ to

$$\Phi_n(\kappa) = 0.033C_n^2 \exp\left[-\kappa^2 \ell_0 / 5.92^2\right] / \left[\kappa^2 + 2\pi / L_0\right]^{11/6}$$

and substituting H in Eq.3.13 $m^2(r, \phi_r, L)$ for Bessel Gauss beam becomes

$$\begin{aligned}
m^2 r, \phi_r, L = & 0.4147 C_n^2 k^2 \int_0^L d\eta \int_0^\infty \kappa d\kappa \int_0^{2\pi} d\phi_\kappa \frac{\exp[-\kappa^2 \ell_0 / 5.92^2]}{[\kappa^2 + 2\pi / L_0^2]^{11/6}} \\
& \times \operatorname{Re} \left\{ \exp \left[-\frac{4\alpha_r \kappa r L - \eta}{1 - 4\alpha_i L + 4|\alpha|^2 L^2} \cos \phi_\kappa - \phi_r \right] \exp \left[-\frac{2\alpha_r \kappa^2 L - \eta^2}{k [1 - 4\alpha_i L + 4|\alpha|^2 L^2]} \right] \right\} \\
& \times J_0 \left\{ \frac{a_B [\kappa^2 L - \eta^2 - 2k\kappa r L - \eta \cos(\phi_\kappa - \phi_r) k^2 r^2]^{1/2}}{k (+2j\alpha L)} \right\} \\
& \times J_0 \left\{ \frac{a_B [\kappa^2 (L - \eta^2) - 2k\kappa r (L - \eta) \cos(\phi_\kappa - \phi_r) k^2 r^2]^{1/2}}{k (-2j\alpha^* L)} \right\} / \left[J_0 \left(\frac{a_B r}{1 + 2j\alpha\eta} \right) J_0 \left(\frac{a_B r}{1 - 2j\alpha^* \eta} \right) \right] \\
& - \exp \left[-\frac{j\kappa^2 (+2j\alpha\eta)(L - \eta)}{k (+2j\alpha L)} \right] J_0 \left\{ \frac{a_B [\kappa^2 (L - \eta^2) - 2k\kappa r (L - \eta) \cos(\phi_\kappa - \phi_r) k^2 r^2]^{1/2}}{k (+2j\alpha L)} \right\} \\
& \times J_0 \left\{ \frac{a_B [\kappa^2 (L - \eta^2) + 2k\kappa r (L - \eta) \cos(\phi_\kappa - \phi_r) k^2 r^2]^{1/2}}{k (+2j\alpha L)} \right\} / \left[J_0 \left(\frac{a_B r}{1 + 2j\alpha\eta} \right) \right]^2
\end{aligned} \tag{3.15}$$

where α_r , α_i and $|\alpha|$ are components of absolute value parameters

3.4 Scattering

This part of the thesis is studied based on [45]. In terms of scattering from the aerosols, it must be examined according to the comparison of wavelength and particle size. Scattering is analyzed into two groups as Mie scattering and nonselective scattering. Mie scattering is valid when wavelength is close to particle size. From the same resource, scattering coefficient can be written as

$$\rho_\lambda = NC\pi r_p^2 \tag{3.16}$$

where C is between 0 and 4, N gives the number of particles, and r_p is the radius of the particle.

As opposed to Mie scattering, nonselective scattering occurs when wavelength is much smaller than the particle size. There are three different effects of nonselective scattering because of the particle size as edge diffraction from the particle, absorbance of the particle, and reflection from the particle. For our case, Mie scattering seems valid because operating wavelength is close to particle size when C is taken as 2.

It is easy to understand above calculations atmosphere is one of the most important factors for a FSO communication system. Commercial systems can break down under heavily fog conditions. To prevent this breaking down situation, FSO systems sometimes can be used as hybrid systems. When BER increases, system automatically activates the RF communication.

3.5 Random Phase Screen Derivation and Its Application for Selected Beam Types

This part is based on the lecture notes on Random Phase Screen by Eyyuboğlu, H.T [48]. At the receiver side, receiver plane field can be written from Huygens-Fresnel Integral as

$$\begin{aligned}
 u_r(r_x, r_y, z) &= \frac{-jk \exp(jkL)}{2\pi L} \int_{-\infty}^{\infty} \int_{-\infty}^{\infty} d^2s u_s(\mathbf{s}) \exp\left[\frac{jk}{2L} (\mathbf{r} - \mathbf{s})^2\right] \quad \text{with } \mathbf{s} = (s_x, s_y), \quad \mathbf{r} = (r_x, r_y) \\
 u_r(r_x, r_y, L) &= \frac{-jk \exp(jkL)}{2\pi L} \int_{-\infty}^{\infty} \int_{-\infty}^{\infty} ds_x ds_y u_s(s_x, s_y) \exp\left\{\frac{jk}{2L} [r_x - s_x]^2 + [r_y - s_y]^2\right\} \\
 &= \frac{-jk \exp(jkL)}{2\pi L} \int_{-\infty}^{\infty} \int_{-\infty}^{\infty} ds_x ds_y u_s(s_x, s_y) \exp\left\{\frac{jk}{2L} [-2s_x r_x - 2s_y r_y + s_x^2 + s_y^2 + r_x^2 + r_y^2]\right\} \quad (3.17)
 \end{aligned}$$

In second representation, exponential inside integral can be divided as

$$u_r(r_x, r_y, L) = \frac{-jk \exp(jkL)}{2\pi L} \exp\left[\frac{jk}{2L} (r_x^2 + r_y^2)\right] \int_{-\infty}^{\infty} \int_{-\infty}^{\infty} ds_x ds_y u_s(s_x, s_y) \exp\left[\frac{jk}{2L} (s_x^2 + s_y^2)\right] \exp\left[-\frac{jk}{L} (s_x r_x + s_y r_y)\right] \quad (3.18)$$

Looking at the last exponential, it is clear that there is a Fourier transform relationship between transmitter and receiver planes in Eq.3.18.

$$u_r(r_x, r_y, L) = \frac{-jk \exp(jkL)}{2\pi L} \exp\left[\frac{jk}{2L}(r_x^2 + r_y^2)\right] \mathbf{F}^{-1}\left\{\mathbf{F}\left[u_s(s_x, s_y)\right] \mathbf{F}\left\{\exp\left[\frac{jk}{2L}(s_x^2 + s_y^2)\right]\right\}\right\} \quad (3.19)$$

\mathbf{F} shows the Fourier transform operator. It is clear that Eq.3.19 is not a classical equation, since it includes one Fourier transform, but offers fixed scaling between the source and receiver plane grid spacing. On the other hand, Eq.3.17 can also be written by applying convolution as

$$u_r(r_x, r_y, L) = \int_{-\infty}^{\infty} \int_{-\infty}^{\infty} ds_x ds_y u_s(s_x, s_y) h(r_x - s_x, r_y - s_y) \quad (3.20)$$

When it is compared Eq.3.17 and Eq.3.20, it is found that h which is the impulse response, can be equated to

$$h(x, y) = \frac{-jk \exp(jkL)}{2\pi L} \exp\left[\frac{jk}{2L}(x^2 + y^2)\right],$$

$$h(r_x - s_x, r_y - s_y) = \frac{-jk \exp(jkL)}{2\pi L} \exp\left\{\frac{jk}{2L}\left[(r_x - s_x)^2 + (r_y - s_y)^2\right]\right\} \quad (3.21)$$

Therefore Eq.3.20 means that

$$u_r(r_x, r_y, L) = u_s(s_x, s_y) \otimes h(r_x, r_y) \quad (3.22)$$

where \otimes indicates the convolution operation. Eq.3.22 does not take us the propagation simulation. That's why; this equation should be examined in detail.

Eq.3.22 can be represented as

$$u_r(r_x, r_y, L) = \mathbf{F}^{-1}\left\{\mathbf{F}\left[u_s(s_x, s_y)\right] \mathbf{F}\left[h(r_x, r_y)\right]\right\} = \mathbf{F}^{-1}\left\{\mathbf{F}\left[u_s(s_x, s_y)\right] H(f_x, f_y)\right\} \quad (3.23)$$

Then, by applying the Fourier Transform of $h(x, y)$ [48], Eq.3.23 turns into

$$\begin{aligned}
\mathbf{F}[h(x, y)] &= H(f_x, f_y) = \exp(jkL) \exp\left[-\frac{2j\pi^2 L}{k} (f_x^2 + f_y^2)\right] \\
&= \exp(jkL) \exp\left[-j\pi\lambda L (f_x^2 + f_y^2)\right]
\end{aligned} \tag{3.24}$$

The only possible case to use Eq.3.23 is that source plane coordinates are the same as receiver plane coordinates, although it is explained in [50]. Otherwise, scaling parameter has to be integrated to it. To realize it, it is set as $\mathbf{r} = m_f \mathbf{s}$ in Eq.3.17.

Defining scaling term

$$\mathbf{r} - \mathbf{s}^2 = m_f \left(\frac{\mathbf{r}}{m_f} - \mathbf{s} \right)^2 - \left(\frac{1 - m_f}{m_f} \right) \mathbf{r}^2 + 1 - m_f \mathbf{s}^2 \tag{3.25}$$

After inserting Eq.3.25 into Eq.3.17, equation becomes

$$u_r(\mathbf{r}, L) = \frac{-jk \exp(jkL)}{2\pi L} \exp\left[\frac{jk}{2L} \left(\frac{m_f - 1}{m_f} \right) \mathbf{r}^2 \right] \int_{-\infty}^{\infty} \int_{-\infty}^{\infty} d^2 \mathbf{s} u_s(\mathbf{s}) \exp\left[\frac{jk}{2L} m_f \left(\frac{\mathbf{r}}{m_f} - \mathbf{s} \right)^2 \right] \exp\left[\frac{jk}{2L} (1 - m_f) \mathbf{s}^2 \right] \tag{3.26}$$

By introducing

$$u_{s1}(\mathbf{s}) = \frac{1}{m_f} u_s(\mathbf{s}) \exp\left[\frac{jk}{2L} (1 - m_f) \mathbf{s}^2 \right] \tag{3.27}$$

Eq.3.26 turns into

$$u_r(\mathbf{r}, L) = \frac{-jk \exp(jkL)}{2\pi L} \exp\left[\frac{jk}{2L} \left(\frac{m_f - 1}{m_f} \right) \mathbf{r}^2 \right] \int_{-\infty}^{\infty} \int_{-\infty}^{\infty} d^2 \mathbf{s} m_f u_{s1}(\mathbf{s}) \exp\left[\frac{jk}{2L} m_f \left(\frac{\mathbf{r}}{m_f} - \mathbf{s} \right)^2 \right] \tag{3.28}$$

By applying the scaling $\mathbf{r}_1 = \mathbf{r}/m_f$, $L_1 = L/m_f$, Eq.3.28 will become

$$u_r(\mathbf{r}, L) = \frac{-jk \exp(jkL)}{2\pi L} \exp\left[\frac{jk}{2L} \left(\frac{m_f - 1}{m_f} \right) \mathbf{r}^2 \right] \int_{-\infty}^{\infty} \int_{-\infty}^{\infty} d^2 \mathbf{s} m_f u_{s1}(\mathbf{s}) \exp\left[\frac{jk}{2L_1} \mathbf{r}_1 - \mathbf{s}^2 \right] \tag{3.29}$$

Here, it must be recognized that scaling is applied inside the integral because the terms out of the integral are constants. Inside of the integral in Eq.3.29 is shown as convolution, but some terms cannot be extracted to outside as in Eq.3.22. Therefore

$$u_r(\mathbf{r}, L) = \exp(jkL) \exp\left[\frac{jk}{2L}\left(\frac{m_f - 1}{m_f}\right)\mathbf{r}^2\right] \int_{-\infty}^{\infty} \int_{-\infty}^{\infty} d^2s m u_{s1}(\mathbf{s}) h(\mathbf{r}_1 - \mathbf{s}) \quad (3.30)$$

where

$$h(\mathbf{r}_1 - \mathbf{s}) = \frac{-jk}{2\pi L} \exp\left[\frac{jk}{2L_1}(\mathbf{r}_1 - \mathbf{s})^2\right] \quad (3.31)$$

After taking the Fourier transform of Eq.3.31, it becomes

$$H(\mathbf{f}) = \mathbf{F}[h(\mathbf{r}_1 - \mathbf{s})] = \exp(-j\pi\lambda z_1 \mathbf{f}^2) = \exp\left(-j\pi\lambda \frac{z}{m_f} \mathbf{f}^2\right) = \exp\left(-\frac{2j\pi^2 z}{m_f k} \mathbf{f}^2\right) \quad (3.32)$$

As a result, it turns in to

$$\begin{aligned} u_r(\mathbf{r}, L) &= \exp(jkL) \exp\left[\frac{jk}{2L}\left(\frac{m_f - 1}{m_f}\right)\mathbf{r}^2\right] u_{s1}(\mathbf{s}) \otimes h(\mathbf{r}_1) \\ &= \exp(jkL) \exp\left[\frac{jk}{2L}\left(\frac{m_f - 1}{m_f}\right)\mathbf{r}^2\right] \mathbf{F}^{-1} \left\{ \mathbf{F}[u_{s1}(\mathbf{s})] \mathbf{F}[h(\mathbf{r}_1)] \right\} \\ &= \exp(jkL) \exp\left[\frac{jk}{2L}\left(\frac{m_f - 1}{m_f}\right)\mathbf{r}^2\right] \mathbf{F}^{-1} \left\{ \mathbf{F}[u_{s1}(\mathbf{s})] \mathbf{F}[h(\mathbf{r}_1)] \right\} \\ &= \exp(jkL) \exp\left[\frac{jk}{2L}\left(\frac{m_f - 1}{m_f}\right)\mathbf{r}^2\right] \mathbf{F}^{-1} \left\{ \mathbf{F}\left[\frac{u_s}{m_f} \exp\left[\frac{jk}{2L}(-m_f \mathbf{s})^2\right]\right] \mathbf{F}[h(\mathbf{r}_1)] \right\} \end{aligned} \quad (3.33)$$

Taking the inverse of spatial coordinates, frequency components of \mathbf{f} can be obtained. If it is set as $m_f = 1$, then Eq. 3.33 reduces to Eq.3.23 above. In the case of

turbulent atmosphere, it is involved the random phase perturbations in Eq.3.33 as follows

$$u_r(\mathbf{r}, L) = \exp(jkL) \exp\left[\frac{jk}{2L}\left(\frac{m_f-1}{m_f}\right)\mathbf{r}^2\right] \overbrace{\exp[\theta(\mathbf{r})]}^{\text{random phase perturbations}} \mathbf{F}^{-1}\left\{\mathbf{F}\left[\frac{u_s(\mathbf{s})}{m_f} \exp\left[\frac{jk}{2L}(1-m_f)\mathbf{s}^2\right]\right] H(\mathbf{f})\right\} \quad (3.34)$$

Eq.3.34 can also be calculated as convolution integral. So, following equations can be derived as

$$u_{s2}(\mathbf{s}) = u_s(\mathbf{s}) \exp\left[\frac{jk}{2L}(1-m_f)\mathbf{s}^2\right] \quad (3.35)$$

$$h(\mathbf{r}-\mathbf{s}) = \exp\left[\frac{jk}{2L}m_f\left(\frac{\mathbf{r}}{m_f}-\mathbf{s}\right)^2\right] = \exp\left[\frac{jk}{2Lm_f}\mathbf{r}-m_f\mathbf{s}^2\right] \quad (3.36)$$

Therefore, received field can be written without Fourier Transform as

$$\begin{aligned} u_r(\mathbf{r}, L) &= \frac{-jk \exp(jkL)}{2\pi L} \exp\left[\frac{jk}{2L}\left(\frac{m_f-1}{m_f}\right)\mathbf{r}^2\right] \exp[\theta(\mathbf{r})] u_{s2}(\mathbf{s}) \otimes h(\mathbf{s}) \\ &= \frac{-jk \exp(jkL)}{2\pi L} \exp\left[\frac{jk}{2L}\left(\frac{m_f-1}{m_f}\right)\mathbf{r}^2\right] \exp[\theta(\mathbf{r})] \int_{-\infty}^{\infty} \int_{-\infty}^{\infty} d^2\mathbf{s} u_{s2}(\mathbf{s}) \exp\left[\frac{jk}{2Lm_f}\mathbf{r}-m_f\mathbf{s}^2\right] \end{aligned} \quad (3.37)$$

From the received field as usual average intensity is obtained as

$$\langle I(\mathbf{r}, z=L) \rangle = \langle u_r(\mathbf{r}, z=L) u_r^*(\mathbf{r}, z=L) \rangle \quad (3.38)$$

Applying this procedure to received field after some distance, average intensity can be written as

$$\begin{aligned} \langle I(r_x, r_y, L) \rangle &= \left(\frac{k}{2\pi L}\right)^2 \exp\left[\frac{jk r^2}{L}\left(\frac{m_f-1}{m_f}\right)\right] \int_{-\infty}^{\infty} \int_{-\infty}^{\infty} \int_{-\infty}^{\infty} \int_{-\infty}^{\infty} ds_{1x} ds_{1y} ds_{2x} ds_{2y} u_s(s_{1x}, s_{1y}) u_s^*(s_{2x}, s_{2y}) \exp\left[\frac{jk}{L}\left(\frac{r-m_f s}{m_f}\right)\right] \\ &\quad \langle \exp[\theta(\mathbf{s}_{1x}, \mathbf{s}_{1y})] \theta^*(\mathbf{s}_{2x}, \mathbf{s}_{2y}) \rangle \end{aligned} \quad (3.39)$$

Because change on receiver plane coordinates is zero, $\exp[\theta(\mathbf{r}, \mathbf{s})]$ term becomes $\exp[\theta(\mathbf{s})]$. The term $\theta \mathbf{r}_1, \mathbf{s}_1 + \theta^* \mathbf{r}_2, \mathbf{s}_2$ is called as wave structure function. Wave structure function is written in Cartesian coordinates as

$$\left\langle \exp\left[\theta_{s_{1x}, s_{1y}} + \theta^*_{s_{2x}, s_{2y}}\right] \right\rangle = \exp\left[-\frac{|\mathbf{s}_1 - \mathbf{s}_2|^2}{\rho_r^2}\right] = \exp\left[-\frac{s_{1x}^2 + s_{2x}^2 + s_{1y}^2 + s_{2y}^2 - 2s_{1x}s_{2x} - 2s_{1y}s_{2y}}{\rho_r^2}\right] \quad (3.40)$$

where ρ_r is the spatial coherence length. Coherence length can be represented as $\rho_r = 0.545C_n^2 k^2 L^{-5/3}$ with C_n^2 is known the structure constant, identifies the turbulence level in the medium. To obtain the received field by feeding the system with Bessel like beams $u_{s_{20}} \mathbf{s}$ can be derived as

$$u_{s_{20}} \mathbf{s} = A_c J_0 a_B s \exp(-jn\phi) \exp\left[\frac{jk}{2L} (1 - m_f) \mathbf{s}^2\right] \quad (3.41)$$

Then, by substituting $u_{s_{20}} \mathbf{s}$ in Eq.3.40 in the place of $u_{s_2} \mathbf{s}$, received field of Bessel beam is analytically derived as

$$\begin{aligned} u_r \mathbf{r}, L &= \frac{-jk \exp(jkL)}{2\pi L} \exp\left[\frac{jk}{2L} \left(\frac{m_f - 1}{m_f}\right) \mathbf{r}^2\right] A_c J_0 a_B s \exp(-jn\phi) \exp\left[\frac{jk}{2L} (1 - m_f) \mathbf{s}^2\right] \otimes h \mathbf{s} \\ &= \frac{-jk \exp(jkL)}{2\pi L} \exp\left[\frac{jk}{2L} \left(\frac{m_f - 1}{m_f}\right) \mathbf{r}^2\right] \int_{-\infty}^{\infty} \int_{-\infty}^{\infty} d^2 \mathbf{s} A_c J_0 a_B s \exp(-jn\phi) \exp\left[\frac{jk}{2L} (1 - m_f) \mathbf{s}^2\right] \exp\left[\frac{jk}{2L m_f} (\mathbf{r} - m_f \mathbf{s})^2\right] \end{aligned} \quad (3.42)$$

For Bessel-Gauss beam $u_{s_{20}} \mathbf{s}$ parameter is derived as

$$u_{s_{20}} \mathbf{s} = A_c J_0 a_B s \exp(-jn\phi) \exp[-k\alpha s^2] \exp\left[\frac{jk}{2L} (1 - m_f) \mathbf{s}^2\right] \quad (3.43)$$

As similar to Bessel beam, received field of Bessel-Gauss beam is obtained substituting in Eq.3.38 as

$$\begin{aligned}
u_r \text{ r,L} &= \frac{-jk \exp jkL}{2\pi L} \exp \left[\frac{jk}{2L} \left(\frac{m_f - 1}{m_f} \right) \mathbf{r}^2 \right] A_c J_0 a_B s \exp(-jn\phi) \exp -k\alpha s^2 \exp \left[\frac{jk}{2L} (1 - m_f) s^2 \right] \otimes h \mathbf{s} \\
&= \frac{-jk \exp jkL}{2\pi L} \exp \left[\frac{jk}{2L} \left(\frac{m_f - 1}{m_f} \right) \mathbf{r}^2 \right] \int_{-\infty}^{\infty} \int_{-\infty}^{\infty} d^2 \mathbf{s} A_c J_0 a_B s \exp(-jn\phi) \exp -k\alpha s^2 \exp \left[\frac{jk}{2L} (-m_f) \mathbf{s}^2 \right] \exp \left[\frac{jk}{2L m_f} (-m_f \mathbf{s}^2) \right] \quad (3.44)
\end{aligned}$$

3.6 Power Settings of The Beam Types

To set power to 21 mW, following equation is hold

$$P_s = \frac{1}{2} \pi \alpha_s^2 \quad (3.45)$$

Three settings are taken into account to generate 21 mW output power such as

$$\begin{aligned}
\alpha_s &= 3.2 \text{ cm and } \alpha_B = 37.61 \text{ where } \alpha_B = 1.2 / \alpha_s \\
\alpha_s &= 6.5 \text{ cm and } \alpha_B = 30.77 \text{ where } \alpha_B = 2 / \alpha_s \\
\alpha_s &= 7.9 \text{ cm and } \alpha_B = 30.76 \text{ where } \alpha_B = 2.43 / \alpha_s
\end{aligned} \quad (3.46)$$

where α_s is the Gaussian source size and α_B is the Bessel function argument. It means that to generate the same amount of power source size is set as above using the Gaussian source size. Above values are tested in MATLAB utilizing Eq.3.45.

3.7 Signal to Noise Ratio Derivation

This part of the thesis is studied in [40]. Signal to noise ratio is one of the important parameter to observe the system performance. As it is stated in basics of FSO part in this thesis, APD generates electrical current according to following formula

$$\langle I_k \rangle = M_f R_f \langle P_r(L) \rangle \quad (3.47)$$

At the receiver side, three types of noise are added to the original signal regarding shot, thermal, and scintillation noise. Shot noise is caused by photodiode itself and it is calculated as below

$$\sigma_{SG}^2 = 2q[M_f R_f \langle P_r(L) \rangle + I_k] B_w \quad (3.48)$$

where I_k is the dark current and B_w is the electrical bandwidth, and q is the electron charge. Next, thermal noise is caused by the load resistor of receiver circuit and it is calculated as below

$$\sigma_{IG}^2 = 4k_B T_K B_w F_N / R_L \quad (3.49)$$

where k_B is the Boltzmann constant, T_K denotes temperature in terms of Kelvin, R_L is the load resistor, and F_N is noise factor. Finally, scintillation noise is calculated as

$$\sigma_{PG}^2 = M_f^2 R_f^2 \left[\langle P_r^2(L) \rangle - \langle P_r(L) \rangle^2 \right] \quad (3.50)$$

SNR is derived by using these types of noise as

$$\text{SNR} = \frac{\text{signal power}}{\text{noise power}} = \frac{P_s}{\sigma_{SG}^2 + \sigma_{IG}^2 + \sigma_{PG}^2} \quad (3.51)$$

At this point, it taken as $P_s = \langle I_f \rangle^2$. After substituting the variables to the equation, it becomes

$$\text{SNR} = \frac{M_f^2 R_f^2 \langle P_r^2(L) \rangle^2}{2q[M_f R_f \langle P_r(L) \rangle + I_k] B_w + 4k_B T_K B_w F_N / R_L + M_f^2 R_f^2 \left[\langle P_r^2(L) \rangle - \langle P_r(L) \rangle^2 \right]} \quad (3.52)$$

In this study, MATLAB simulations were performed using Eq.3.42 and Eq.3.44. Truncated Bessel and Bessel-Gauss beams were propagated through random phase screen in MATLAB environment. At the transmitter powers of the beams are set equally to 21 mW. Results of BER, SNR, and received power values are analyzed

with respect to C_n^2 . Even if output power is set to 21 mW, because of random phase fluctuations received power can change randomly in the atmosphere.

CHAPTER 4

ANALYSIS WITH RESPECT TO SOURCE SIZE

4.1 Pe, SNR, Received Power Analysis of Bessel Gauss Beam when $\alpha_s = 3.2\text{cm}$

In this part of the study, results of simulations which were performed in MATLAB are analyzed.

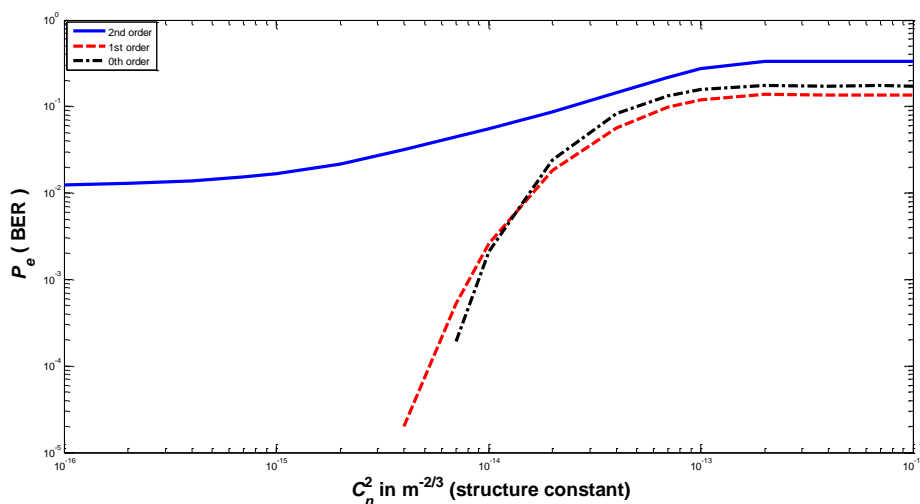


Figure 12 Pe behavior of Bessel Gauss Beams (BGBs) with respect to structure constant when $\alpha_s = 3.2\text{cm}$ for different orders.

Fig.12 shows the Pe comparison of Bessel Gauss Beams (BGBs) with different orders when $\alpha_s = 3.2\text{cm}$ with respect to the structure constant. When structure constant decreases as in free space, which occurs between satellites, Pe converges to 10^{-5} for all beam orders. As compared to free space, BER performances of the beam changes in turbulent atmosphere. In this case, BGB of first kind shows the best BER performance which is in between 2×10^{-2} and 5×10^{-1} . BGB of second kind second kind is the worst as it is seen on the graph. Its BER value is approximately 4×10^{-1}

which is not acceptable for successful communication. BGB of zero order locates between first and second kind.

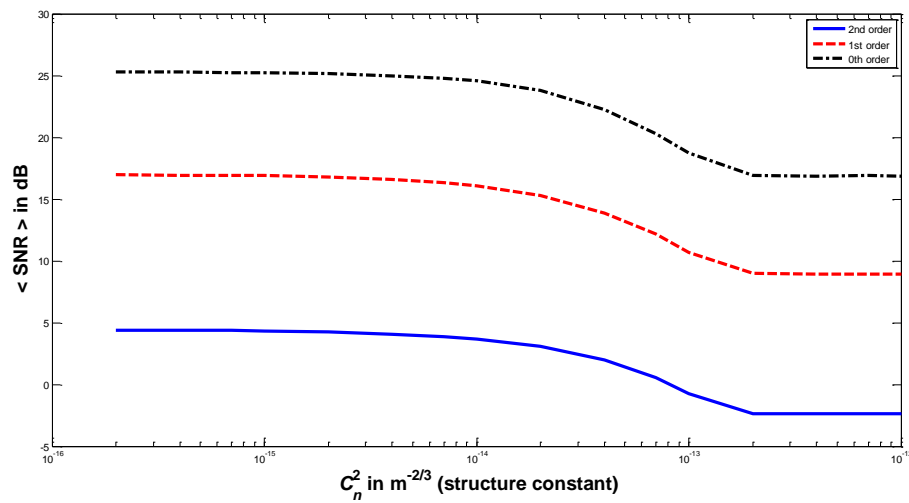


Figure 13 SNR behavior of BGBs with respect to structure constant when $\alpha_s = 3.2\text{cm}$ for different orders.

It is seen on Fig.13 that SNR comparisons of BGBs with different orders. In terms of SNR, second order shows the worst performance even if it is in free space. After a quite big difference, among the SNR values of first and second order beam, first order beam has the second best SNR performance. For small size BGBs, zero order beam shows the best SNR performance as it is seen from the graph.

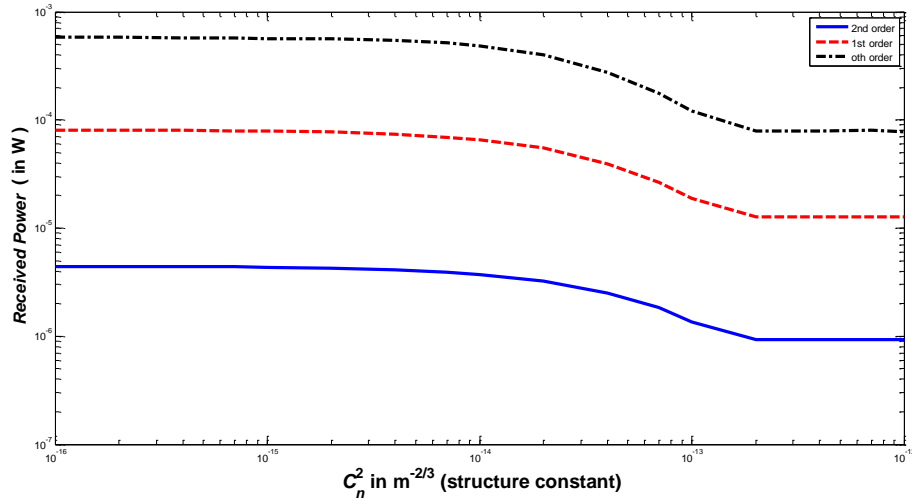


Figure 14 Received power of BGBs with respect to structure constant when $\alpha_s = 3.2\text{cm}$ for different orders.

Fig.14 indicates the received power comparison of BGB when $\alpha_s = 3.2\text{cm}$. As similar to SNR comparison, second order BGB is the worst in both free space and turbulent atmosphere. As opposed to second order, zero order BGB shows the best performance in terms of received power. First order, BGB is located somewhere between zero and second order beams. It is easy to see that received power decreases exponentially when structure constant increases. As it is seen from the figure, beams lose 10 times of its power from free space to turbulent atmosphere.

4.2 Pe, SNR, Received Power Analysis of Bessel Gauss Beam when $\alpha_s = 6.5\text{cm}$

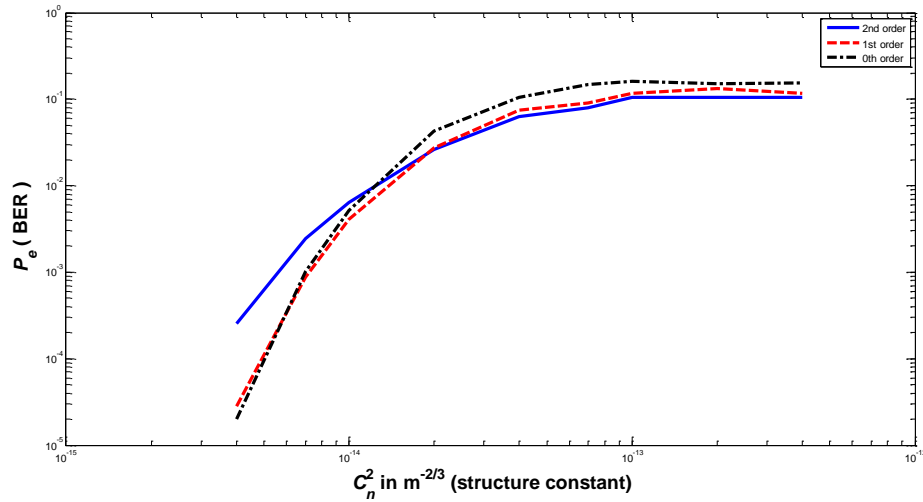


Figure 15 Pe behavior of BGBs with respect to structure constant when $\alpha_s = 6.5\text{cm}$ for different orders.

Fig.15 shows the Pe behaviors of BGBs with $\alpha_s = 6.5\text{ cm}$. When close to free space, best BER performance can be seen by zero order Bessel Gauss Beam which has a Pe value nearly 10^{-5} . First order BGB behaves as similar to zero order BGB but first order beam has higher Pe value. As compared to zero order BGB, second order BGB shows the worst performance in free space region. In turbulent region, roles of the beams change as second order BGB shows the best Pe performance. As compared to free space region, zero order BGB has the worst Pe performance. Again in turbulent region, first order BGB stays between zero and second order beams.

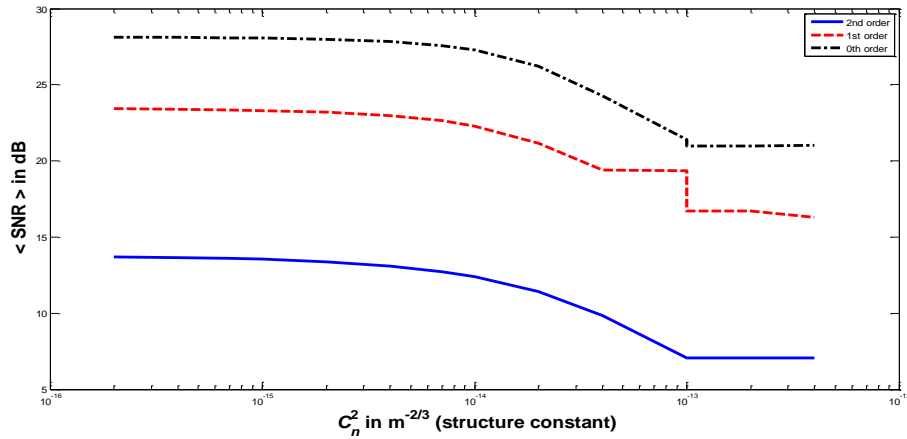


Figure 16 SNR behavior of BGBs with respect to structure constant when $\alpha_s = 6.5\text{cm}$ for different orders.

As seen from Fig.16, both in free space and turbulent atmosphere, second order BGB shows the worst SNR performance. As opposed to second order, zero order BGB shows the best SNR performance. Finally, first order BGB stays between second and zero order BGB. Another inference from this figure is that SNR value decreases approximately 4dB from free space to turbulent atmosphere.

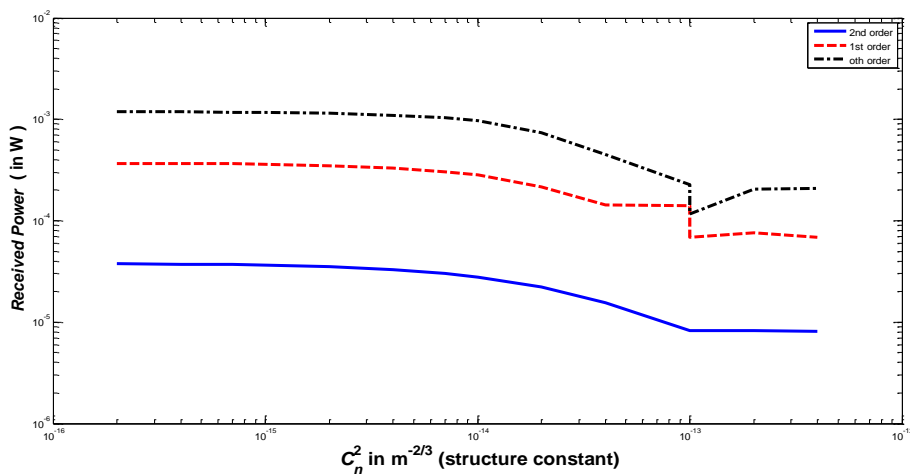


Figure 17 Received power of BGBs with respect to structure constant when $\alpha_s = 6.5\text{cm}$ for different orders.

Fig.17 is similar to Fig.16 which shows SNR comparison of the beams. In terms of received power, second order is the worst, zero order is the best, and first order BGB is somewhere in between as similar to Fig.16. There is a ten times difference between second and zero order beams. Again as similar to SNR, received power decreases in turbulent medium.

4.3 Pe, SNR, Received Power Analysis of Bessel Gauss Beam when $\alpha_s = 7.9\text{cm}$

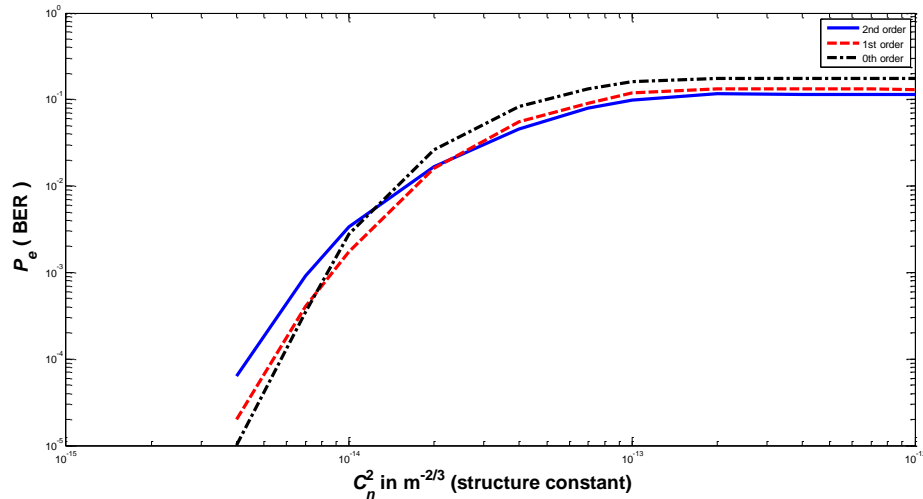


Figure 18 Pe behavior of BGBs with respect to structure constant when $\alpha_s = 7.9\text{cm}$ for different orders.

As it is seen from Fig.18, in free space region, zero order BGB has the lowest Pe value. It means that this beam is the best among the others. At the same environment, second order BGB is the worst in terms of Pe. As compared to zero order and second order, first order BGB is somewhere between them. In turbulent medium, zero order beams is the worst. Different from the free space, here second order BGB has the lowest Pe value. First beam stays between them.

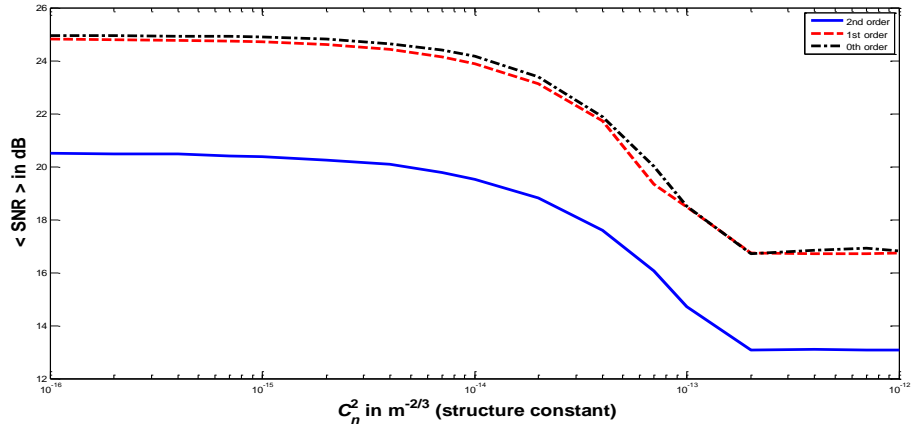


Figure 19 SNR behavior of BGBs with respect to structure constant when $\alpha_s = 7.9\text{cm}$ for different orders.

As it is seen from Fig.19, zero order BGB has the highest SNR value. First order BGB is in the second place even though its SNR value is close to zero order BGB. While zero and first order BGB are in the level of 25 dB, second order BGB is in 20 dB level. This sequence is valid for both free space and turbulent medium. But when come to turbulent medium, SNR value of beams decreases almost 6 dB.

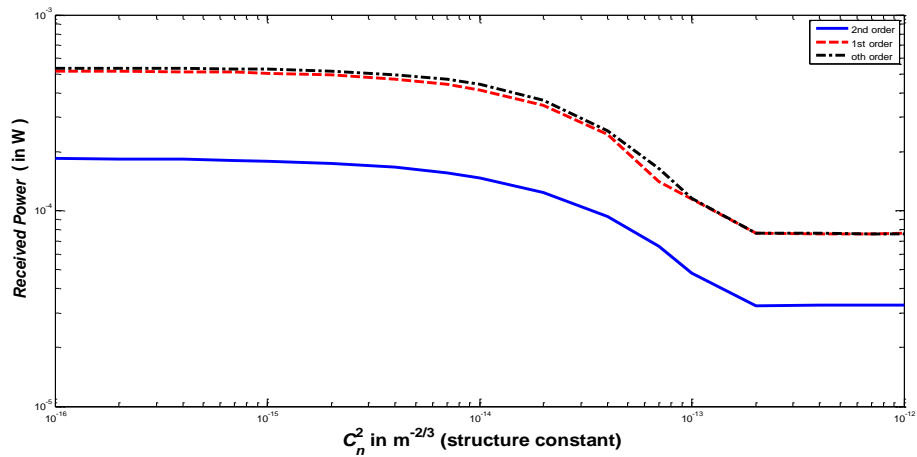


Figure 20 Received power of BGBs with respect to structure constant when $\alpha_s = 7.9\text{cm}$ for different orders.

This graph is similar to Fig.20. The highest received power can be seen by zero order BGB and received power of first order BGB is close but still less than zero order. Finally, received power of the second order BGB is drastically less than the others. As the same as other figures received power in turbulent medium decreases.

CHAPTER 5

ANALYSIS WITH RESPECT TO ORDERS

In this part of the thesis, simulation results according the orders are studied. First, Pe performance of BGB takes place.

5.1 Pe Analysis of Bessel Gauss Beam with respect to the orders

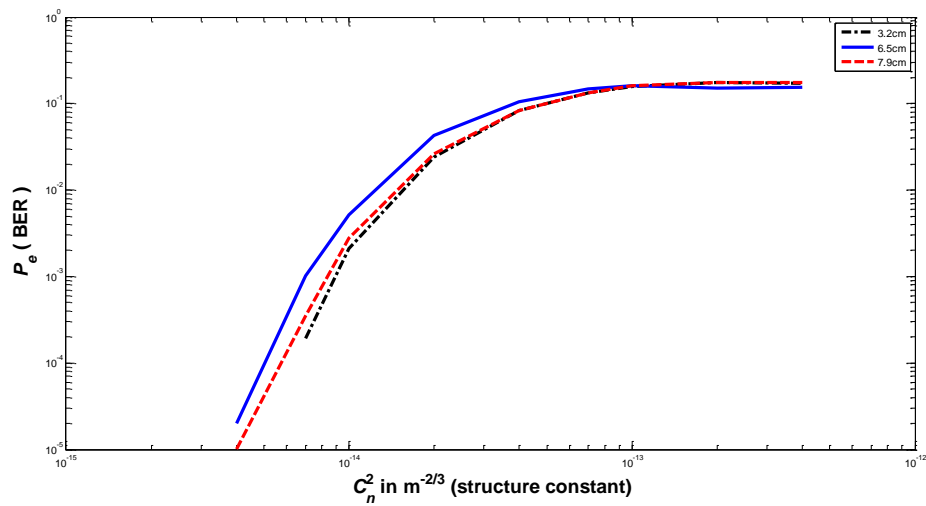


Figure 21 Pe performance of zero order BGB for different source sizes.

Fig.21 illustrates the Pe comparison of zero order BGB. In this figure, it is easy to see that small source size beam has the lowest Pe in both turbulent medium and free space. The highest Pe value can be observed by middle size beam. Middle size beam has the worst performance in terms of Pe in both turbulent atmosphere and free space. Large size beam is located in between them.

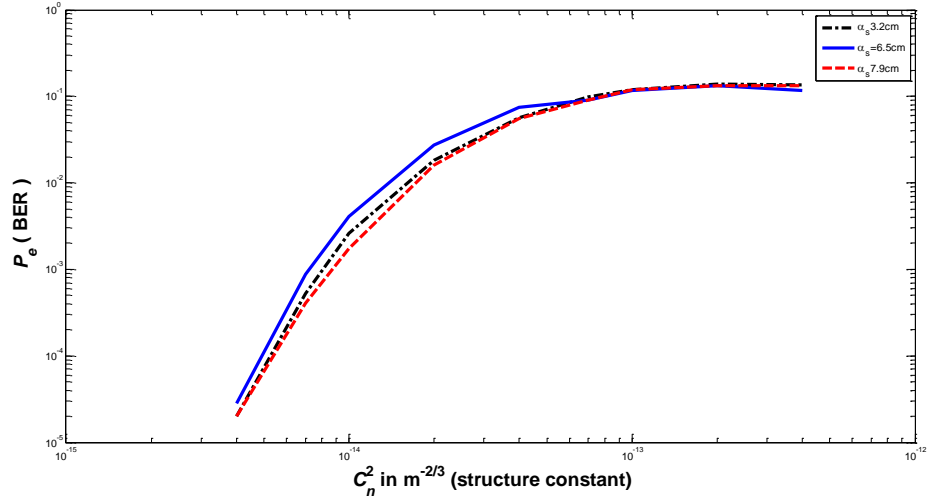


Figure 22 Pe performance of first order BGB for different source sizes.

Figure 22 shows the Pe comparison of first order BGB for different source sizes. For all atmospheric conditions large source size beams shows the best Pe performance. The worst Pe performance of first order BGB can be seen when $\alpha_s = 6.5$ cm. Pe performance of small source size BGB is between them.

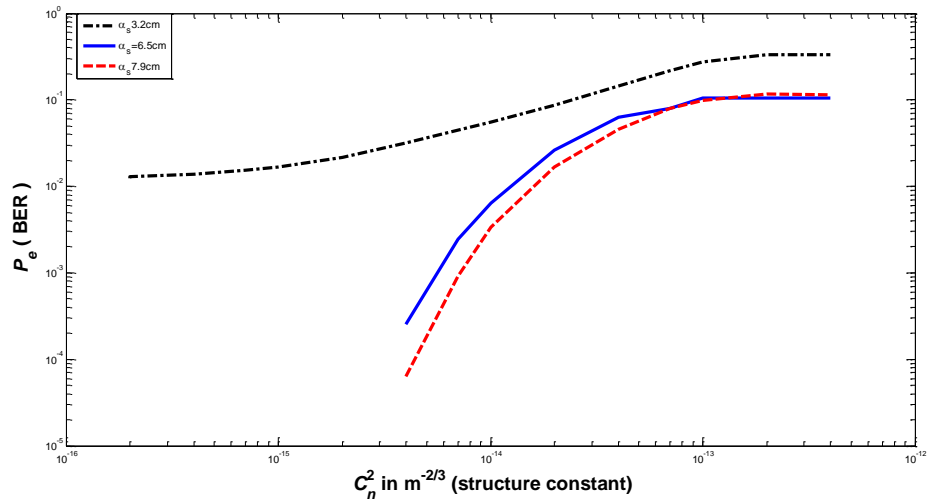


Figure 23 Pe performance of second order BGB for different source sizes.

Pe performance of second order BGB is shown in Fig.23. In this case small source size beam has the highest Pe value. At the other point of view, large size beam has the best Pe performance in all horizontal axes. Additionally, middle source sized beam is placed in between them. For second order BGB, usage large source size beam is seen as advantageous.

5.2 SNR Analysis of Bessel Gauss Beam with respect to the orders

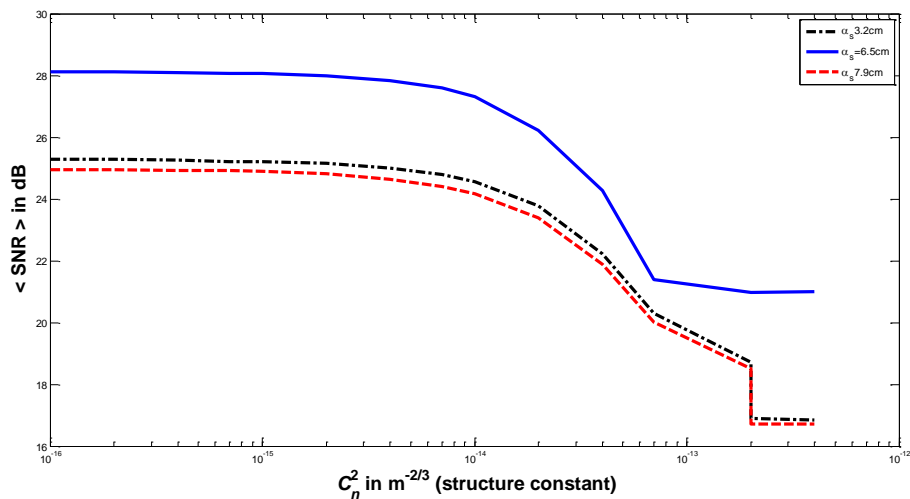


Figure 24 SNR comparison of zero order BGB with different source sizes.

Figure 24 indicates that middle size ($\alpha_s = 6.5$ cm) BGB has the best SNR performance among the zero order BGBs. The lowest SNR value after 5500 meter distance can be seen by the BGB having the largest source size. Small size ($\alpha_s = 3.2$ cm) BGB is a little bit better than the large source size beam but there is still approximately 3 dB difference with middle size beam. As close to turbulent region, SNR decreases approximately 3-4 dB.

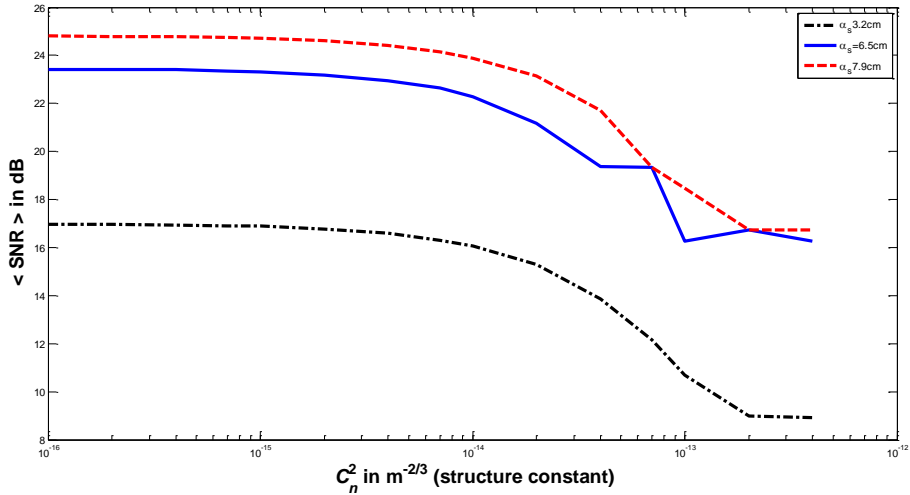


Figure 25 SNR comparison of first order BGB with different source sizes.

Figure 25 represents the SNR comparison of first order BGBs. In this case, large size ($\alpha_s = 7.9$ cm) BGB has the highest SNR value. Different from the previous figure, small source size beam has the lowest SNR value. SNR of middle source size beam is closer to the beam with larger source size. Change in SNR for first order BGB from free space to turbulent atmosphere is 2-3 dB.

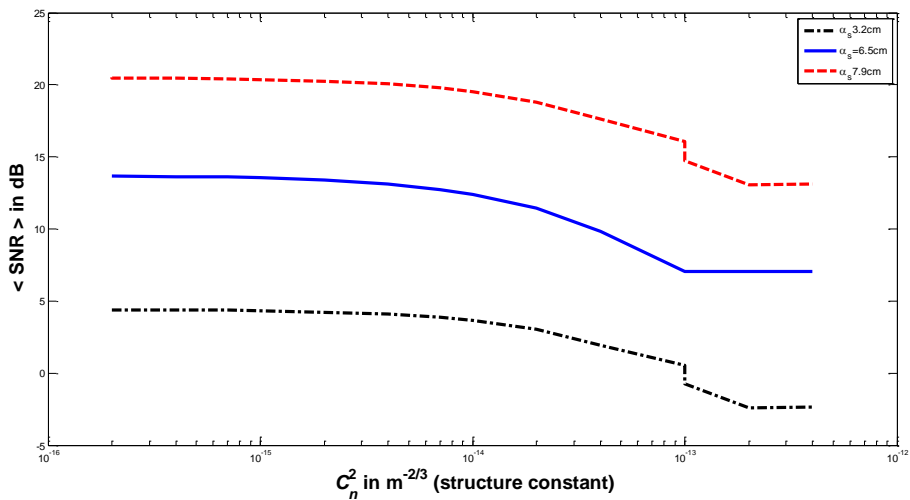


Figure 26 SNR comparison of second order BGB with different source sizes.

As similar to Fig.26, the best SNR performance can be seen by larger source size beam. Middle source size beam follows it decreasing approximately 7 dB. The worst SNR performance can be assigned to small source size beam. As compared to first order BGB, it loses approximately 12 dB less.

5.3 Received Power Analysis of Bessel Gauss Beam with respect to the orders

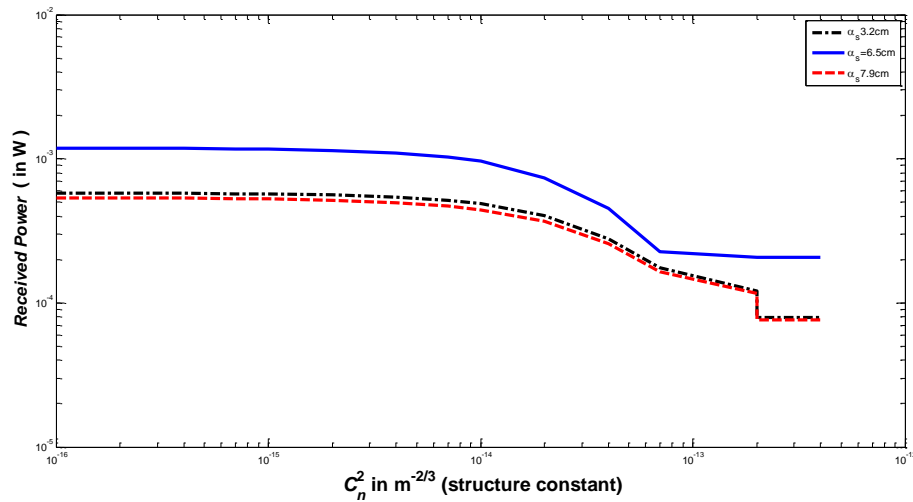


Figure 27 Power comparison of zero order BGB with different source sizes.

Similar view is seen on Fig.27, because middle source size beam provides the highest received power. The lowest power at the receiver after 5500 meter can be measured when the largest source sized beam is used. Small source size beam is better than the larger source size beam.

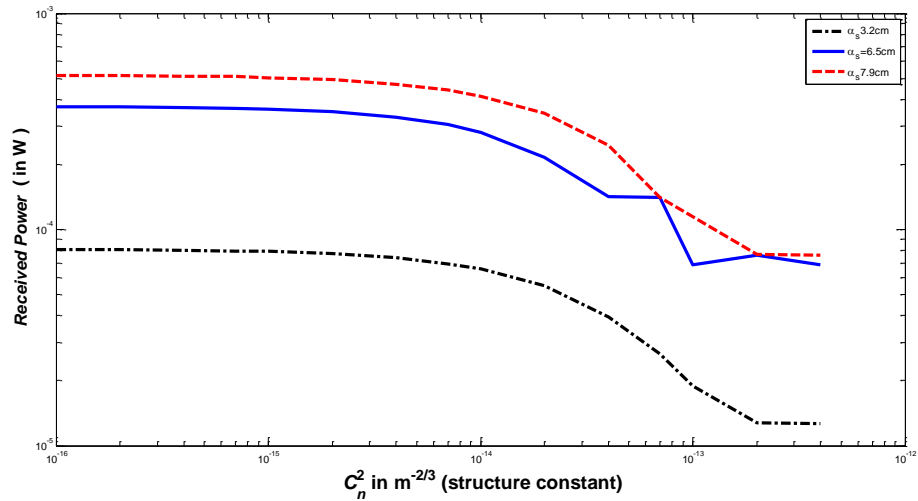


Figure 28 Power comparison of first order BGB with different source sizes.

Figure 28 is also similar to figure of SNR comparison of first order BGMs. However small source size BGB provides the lowest power at the receiver, the largest source sized beam provides the highest power over the receiver. At this time, usage of middle size beam gives closer received power to the best one.

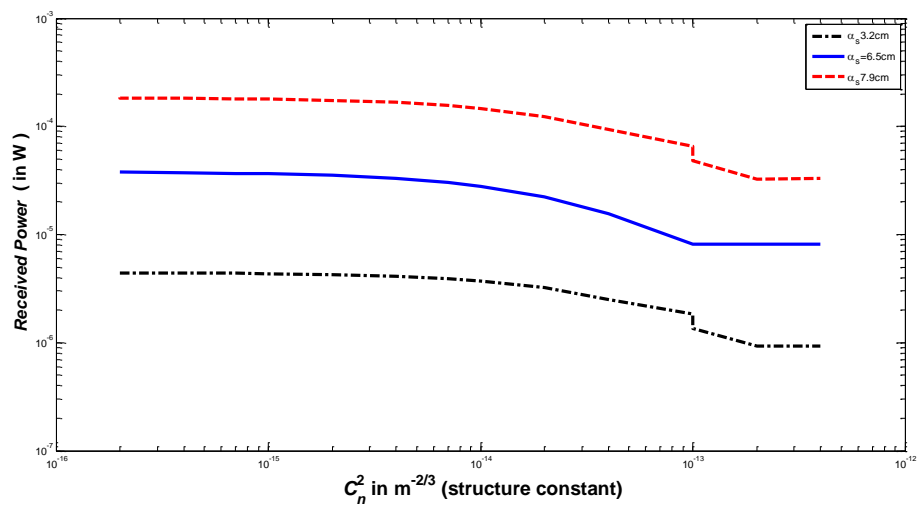


Figure 29 Power comparison of second order BGB with different source sizes.

Figure 29 seems similar to SNR comparison of second order BGB. Again, large source size beam provides highest power over the receiver. In sequence, middle size beam takes the second place and small source size beam shows the worst effort.

CHAPTER 6

ANALYSIS OF TRUNCATED BESSEL BEAM WITH RESPECT TO ORDERS

As it is seen from Fig.30, second order Bessel beam shows the best Pe performance as compared to the zero and first order beams. At this point first order beam has the highest Pe value. When structure constant is close to turbulent atmosphere, zero order beams has the highest Pe value and second order beam shows the best Pe performance.

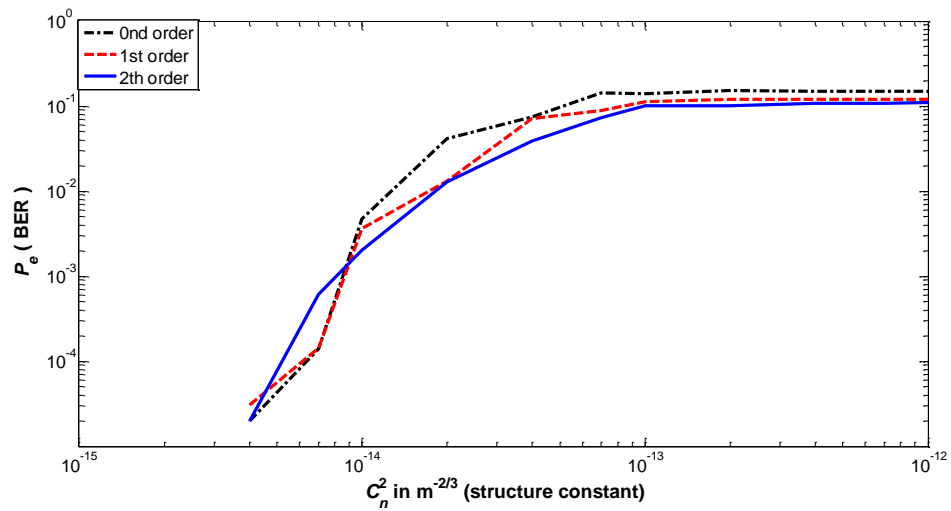


Figure 30 Probability of error comparison of Bessel Beams with different orders.

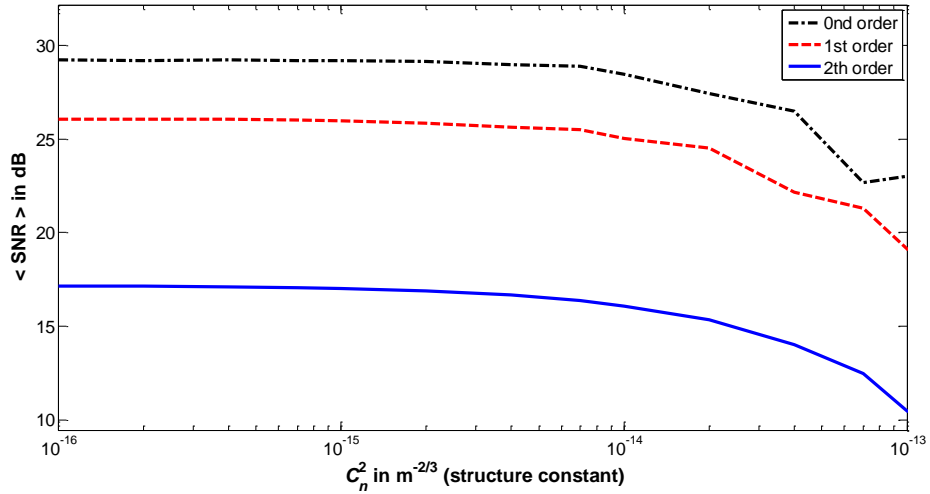


Figure 31 SNR comparisons of Bessel Beams with different orders.

As shown in Fig.31 In terms of SNR, zero order beam has the highest SNR at the receiver even in free space and turbulent atmosphere. As opposed to zero order beam, second order beam has the lowest SNR value at the receiver in somewhere between 15-20 dB. Finally, first order Bessel beam is close but still less than zero order.

CHAPTER 7

CONCLUSION

In this thesis, mainly performance comparison of truncated Bessel and Bessel-Gauss beams were studied. As performance parameter, probability of error, received power and signal to noise ratio are taken into account. To calculate first parameter which is probability of error, error counting is chosen. In this technique, transmitted symbols are stored as an array. At the receiver, receiver symbols are obtained using threshold detection and they are also stored in an array. Finally, both transmitted symbol array and received symbol array are compared. In 100000 symbols, symbols with error are counted and dividing this number to number of transmitted symbols probability of error is derived. Secondly, received power is calculated using Huygens-Fresnel Integral. Huygens-Fresnel Integral gives the received field at the receiver after some distance and turbulent medium. Multiplying received field with its conjugate intensity at the receiver is obtained. Finally, power is calculated by taking the integral of the intensity over the receiver plane. Signal to noise ratio is the last but the not least parameter considered in this thesis. To derive SNR, received power is used because received power is in nominator of SNR. As noise, shot and thermal noise is taken into account to place in the denominator of SNR. Shot noise is the noise caused by photodiode creating the current and thermal noise is the noise caused by the load resistor to generate voltage from current. Dependence of all parameters listed above is analyzed versus structure constant which gives the intensity of atmosphere. All related graphs are plotted and comparison in derived depending on three different Bessel order and source sizes. To understand the working principle of free space optical systems, an optical communication system is designed practically. It is very helpful to get the idea of the system and see the noise over the signals.

To generalize the results of the study, for both beam types received power and SNR value decreases from free space to turbulent atmosphere meaningfully from low structure constant to higher one. Because, atmospheric affects such as attenuation, scattering, scintillation feel over the beam at the receiver. For each beam type SNR value decreases approximately 5 dB during this medium change. In terms of probability of error, this communication system operates better in free space as compared to turbulent region. When 5.5 km link distance and the system with 21 mW output power is considered probability of error for Bessel type beams is close to 10^{-6} level in free space. In turbulent region this number rises to 10^{-2} level. When these numbers are compared with the study in [51], the results seems similar even if output power of the systems are different. This thesis shows that similar BER and SNR results can be obtained applying truncated Bessel and Bessel Gauss beams to FSO systems. Generating these types of beams performance of free space optical communication system can be increased. Furthermore, second order Bessel-Gauss beams show the best probability of error performance in turbulent atmosphere for middle and large source size beams. For the small source size beam second order beam has the worst probability of error performance while first order beam has the best. On the other hand, second order Bessel-Gauss beam has the highest SNR and directly proportional to received power value for all source size beams. In the other point of view, using small source beam lower probability of error values can be obtained among zero, first, and second order Bessel-Gauss beams.

When truncated Bessel and Bessel-Gauss beams are compared in terms of P_e and SNR, similar results are seen. Both truncated Bessel beam and Bessel-Gauss beams with all source sizes show similar P_e performance during turbulent region. In free space region, except small source size Bessel-Gauss beam, they have similar P_e performance. In terms of SNR, large source size Bessel-Gauss beams show the similar SNR performance with truncated Bessel beam. Small and middle source size beams have less SNR value than truncated Bessel beam. Consequently, using truncated Bessel and Bessel-Gauss beam lower P_e values and higher SNR values can

be obtained. It means that applying these beams performance of free space optical systems can be increased.

REFERENCES

1. **Mahdieh M. H. and Pournoury M., (2010)**, “*Atmospheric turbulence and numerical evaluation of bit error rate (BER) in free-space communication*”, Opt. Laser Technol., vol. 42, pp. 55-60.
2. **Chaman –M. A., Ahmadi V., Ghassemlooy Z.,(2010)**, “*A modified model of the atmospheric effects on the performance of FSO links employing single and multiple receivers*”, J. Modern Opt., vol. 57, no.1, pp.37-42.
3. **Andrews L. C. and Philips R. L.,(2004)**, “*Free space optical communication link and atmospheric effects: single aperture and arrays*” in Proceedings of SPIE, Free-Space Laser Communication Technologies XVI, San Jose, Canada, vol. 5338.
4. **Lyke S. D., Voelz D. G., Roggemann M. C., (2009)**, “*Probability density of aperture-averaged irradiance fluctuations for long range free space optical communication links*”, Appl. Opt. vol. 48, pp. 6511-6527.
5. **Toselli I., Andrews L. C., Philips R. L., Ferrero V., (2008)**, “*Free-space optical system performance for laser beam propagation through non-Kolmogorov turbulence*”, Opt. Eng. vol. 47, pp.
6. **Kaisaleh K., (2006)**, “*Performance of Coherent DPSK Free-Space Optical Communication Systems in K-Distributed Turbulence*”, IEEE Trans. Commun. vol. 54, pp. 604-607.
7. **Anguita J. A., Djordjevic I. B., Neifeld M. A., Vasic B. V., (2005)**, “*High-Rate Error-Correction Codes for the Optical Atmospheric Channel*” in Proceedings of SPIE, Free-Space Laser Communications V, Washington, USA, pp.
8. **Djordejevic I. B., Djordjevic G. T., (2009)**, “*On the communication over strong atmospheric turbulence channels by adaptive modulation and coding*”, Opt. Express, vol. 17, pp. 18250-18262.
9. **Luna R., Borah D.K., Jonnalagadda R., Voelz D. G., (2009)**, “*Experimental Demonstration of a Hybrid Link for Mitigating Atmospheric Turbulence Effects in Free-Space Optical Communication*”, IEEE Photon. Technol. Lett., vol 21, no. 17, pp. 1196-1198.
10. **Ren Y., Huang H., Xie G., Ahmed N., Yan Y., Erkmen B. I., Chandrasekaran N., Lavery M. P. J., Steinhoff N. K., Tur M., Dolinar S., Neifeld M., Padgett M. J., Boyd R. W., Shapiro J. H., Willner A. E., (2013)**, “*Atmospheric turbulence effects on the performance of a free space optical link employing orbital angular momentum multiplexing*”, Opr. Lett., vol. 38, no. 20, pp.4062-4065.
11. **PoPoolala W. O., (2009)**, “*BPSK Subcarrier Intensity Modulated Free-Space Optical Communications in Atmospheric Turbulence*”, J. Lightw. Technol., vol. 27, no.8, pp. 967-973.

12. **Wang Z., Zhong W. –D., Fu S., Lin C., (2009)**, “*Performance Comparison of Different Modulation Formats Over Free-Space Optical (FSO) Turbulence Links With Space Diversity Reception Technique*”, IEEE Photon. J., vol. 1, no. 6, 276-285.
13. **Chafiq A., Hricha Z., Belafhal A., (2005)**, “*Paraxial propagation of Mathieu beams through an apertured ABCD optical system*”, Opt. Commun., vol. 253, 223-230.
14. **Chafiq A., Hricha Z., Belafhal A., (2006)**, “*A detailed study of Mathieu–Gauss beams propagation through an apertured ABCD optical system*”, Opt. Commun., vol. 265, pp. 594-602.
15. **Ricklin J. C., (2003)**, “*Atmospheric optical communication with a Gaussian Schell beam*”, J. Opt. Soc. Am. A, vol. 20, no. 5, 856-866.
16. **Jiang Z. –P., (1996)**, “*Super-Gaussian-Bessel beam*”, Opt. Commun., vol. 125, 207-210.
17. **Gori F., Guattari G., Padovani C., (1987)**, “*Bessel-Gauss Beams*”, Opt. Commun., vol. 64, no. 6, pp. 491-495.
18. **Bayraktar M. and Başdemir H. D., (2014)** “*Cylindrical-Sinc Beam*”, Optik, vol. 125, pp. 5869-5871.
19. **Durnin J., (1987)**, “*Exact solutions for nondiffracting beams. I. The scalar theory*”, J. Opt. Soc. Am. A, vol. 4, no. 4, 651-654.
20. **Chavez-Cerda S., McDonald G. S., New G. H. C., (1996)**, “*Nondiffracting beams: travelling, standing, rotating and spiral waves*”, Opt. Commun., vol. 123, 225-233.
21. **Williams W. B., Pendry J. B., (2005)**, “*Generating Bessel beams by use of localized modes*”, J. Opt. Soc. Am. A, vol 22, no. 5, pp. 992-997.
22. **Sun Q., Zhou K., Fang G., Liu Z., Liu S., (2010)**, “*Generation of spiraling high-order Bessel beams*”, Appl Phys B, vol. 104, no. 1, pp.215-221.
23. **Chakraborty R., Ghosh A., (2006)**, “*Generation of an elliptic Bessel beam*”, Opt. Lett., vol. 31, no.1, pp. 38-40.
24. **Anguiano-Morales M., Salas-Peimbert D.P., Trujillo-Schiaffino G., Monzon-Hernández D., Toto-Arellano N. –I., (2011)**, “*Bessel beam spatially truncated*”, Opt. Commun., vol. 284, pp. 1504-1509.
25. **Eyyuboğlu H. T., Voelz D., Xiao X., (2013)**, “*Scintillation analysis of truncated Bessel beams via numerical turbulence propagation simulation*”, Appl. Opt., vol. 52, No. 33, pp. 8032-8039.
26. **Sogomonian S., Klewitz S., Herminghaus S., (1997)**, “*Self-reconstruction of a Bessel beam in a nonlinear medium*”, Opt. Commun., vol. 139, pp. 313-319.

27. **Eyyuboğlu H. T. and Hardalaç F.,(2008)**, “*Propagation of modified Bessel-Gaussian beams in turbulence*”, Opt. Laser Technol., vol. 40, no.2, pp. 343- 351.
28. **Cang J. and Zhang X., (2010)**, “*Axial intensity distribution of truncated Bessel–Gauss beams in a turbulent atmosphere*”, Optik, vol. 121, pp. 239-245.
29. **Wang X. and Lü B.,(2002)**, “*The beam propagation factor and far-field distribution of Bessel-modulated Gaussian beams*”, IEEE J. Quantum Electron, vol. 34, no.11, pp.1071-1077.
30. **Li J., Chen Y., Cao Q., (2013)**, “*Analytical vectorial structure of Bessel–Gauss beam in the near field^P*”, Opt. Laser Technol., vol. 45, pp. 734-747.
31. **Zhang B., Chu X., Wen Q., Zeng Q., (2004)**, “*Approximate method for calculating the generalized beam propagation factor of truncated beams*”, Opt. Commun., vol. 229, pp. 1-10.
32. **Borghi R. and Santarsiero S., (1997)**, “ *M^2 factor of Bessel–Gauss beams*”, Opt. Lett., vol. 22, No. 5, pp. 262-264.
33. **Zhang Z., Pu J., Wang X., (2008)**, “*Focusing of partially coherent Bessel–Gaussian beams through a high-numerical aperture objective*”, Opt. Lett., vol. 33, No. 1, pp. 49-51.
34. **Mei Z. and Zhao D., (2007)**, “*Generalized beam propagation factor of hard-edged circular apertured diffracted Bessel–Gaussian beams*”, Opt. Laser Technol., vol. 39, No. 7, pp. 1389-1394.
35. **Tovar A. A., (2000)**, “*Propagation of Laguerre-Bessel Gaussian beam*”, J. Opt. Soc. Am. A, vol. 17, No. 11, pp. 2010-2018.
36. **Liu D. and Zhou., (2010)**, “*Propagation and the kurtosis parameter of Gaussian flat-topped beams in uniaxial crystals orthogonal to the optical axis*”, Opt. Lasers Eng. Vol. 48, No. 1, pp. 58-63.
37. **Mao H., Ge F., Chen L., Shi X., (2013)**, “*The influence of the bandwidth on beam propagation factor and kurtosis parameter for a broadband beam modulated by a hard-edged aperture*”, Optik, vol. 124, No. 18, pp. 3651-3654.
38. **Luo S. and Lü B.,(2003)**, “ *M^2 factor and kurtosis parameter of super-Gaussian beams passing through an axicon*”, Optik, vol. 114, No. 5, pp. 193-198.
39. **Martinez-Herrero R., Piquero G., Mejias P. M., (1995)**, “*On the propagation of the kurtosis parameter of general beams*”, Opt. Commun., vol. 115, No.3-4, pp. 225-232.
40. **Eyyuboğlu H. T. and Bayraktar M.,(2015)**, “*SNR bounds of FSO links and its evaluation for selected beams*”, J. Modern Opt. vol. 62, no. 16, pp. 1316-1322.

41. **Bloom S., Korevaar E., Schuster J., Willebrand H., (2003)**, “*Understanding the performance of free-space optics [Invited]*”, J. Opt. Netw., vol. 2, no. 6, pp.178-200.
42. Notes on Free Space Propagation by Eyyuboğlu from ece492.cankaya.edu.tr
43. Datasheet of BM03-M-B.
44. Datasheet of AC508.
45. **Blaunstein N., Arnon S., Zilberman A., Kopeika N., (2009)**, “*Applied Aspects of Optical Communication and Lidar*”, CRC Press, New York.
46. **Gradshteyn I. S. and Ryzhik I. M., (2014)**, “*Table of Integrals, Series and Products*”, Academic Press, Massachusetts.
47. **Gradshteyn I. S. and Ryzhik I. M., (2014)**, “*Table of Integrals, Series and Products*”, Academic Press, Massachusetts.
48. **Andrews L. C. and Philips R. L., (2005)**, “*Laser Beam Propagation through Random Media, Second Edition*”, SPIE Press, Washington.
49. **Gradshteyn I. S. and Ryzhik I. M., (2014)**, “*Table of Integrals, Series and Products*”, Academic Press, Massachusetts.
50. **Schmidt J.D., (2010)**, “*Numerical Simulation of Optical Wave Propagation with Examples in MATLAB*”, SPIE, Washington, USA.
51. **Eyyuboğlu H.T., (2014)**, “*Bit error rate analysis of Gaussian, annular Gaussian, cos Gaussian, and cosh Gaussian beams with the help of random phase screen*”, Appl. Opt., vol. 53, No. 17, pp. 3758-3763.
52. **Andrews L. C., (2004)** “*Free space optical communication link and atmospheric effects: single aperture and arrays*”, In Proceedings of SPIE, Free-Space Laser Communication Technologies XVI, Washington, USA,

APPENDICES A

CURRICULUM VITAE



PERSONAL INFORMATION

Surname, Name: Bayraktar, Mert

Date and Place of Birth: 25 March 1990, Samsun

Marital Status: Single

Phone: +90 554 247 72 73

Email: mbayraktar@cankaya.edu.tr

EDUCATION

Degree	Institution	Year of Graduation
B.Sc.	Çankaya Univ., Electronic and Communication Engineering	2013
B.Sc	Çankaya Univ., Computer Engineering (Double Major)	2013
High School	Tülay Başaran High School	2008

WORK EXPERIENCE

Year	Place	Enrollment
2014 - Present	Lazersan Haberleşme	Co-Founder
2013- Present	Çankaya Univ.	Research Assistant

	Electronic and Communication Engineering	
2013 - Present	Lazersan Elektronik	Co-Founder
2012 July	Mikes	Intern
2012 June	Havelsan	Intern
2011 June	Türk Telecom.	Intern
2009 July	Walt Disney World	Life Guard

FOREIN LANGUAGES

Advanced English, Beginner Spanish, Beginner German

PUBLICATIONS

1. Eyyubođlu H.T and Bayraktar M., “SNR bounds of FSO links and its evaluation for selected beams”, J.Mod. Opt., vol 62. No 16, pp. 1316-1322, (2015).
2. Bayraktar, M., Bařdemir, H. D., “*Cylindrical-Sinc Beam*”, OPTIK, vol. 138, pp. 571-584, (2013).

PROJECTS

1. Visible Light Communication System, Project Number: 0082.TGSD.2014, Ministry of Science, Industry and Technology, 2014.
2. Free Space Optics Modem, Project Number: 0935.TGSD.2013, Ministry of Science, Industry and Technology, 2013.

HONOURS AND AWARDS

1. “Yeni Fikirler Yeni İşler 2014“ competition
2st degree in category of Energy
2. “Yeni Fikirler Yeni İşler 2013“ competition
1st degree in category of Defence Industry
3. “Yeni Fikirler Yeni İşler 2013 “ competition
2st degree in category of Information Technology

4. Graduate High Honor Student 2013
Çankaya University

HOBBIES

Travel, Books, Swimming, Fitness